Heliyon 10 (2024) e34740

Contents lists available at ScienceDirect

Heliyon

journal homepage: www.cell.com/heliyon

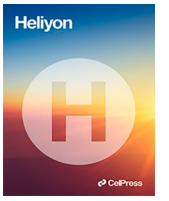

Research article

Research on fruit picking test of blueberry harvesting machinery under transmission clearance

Xiaomeng Lyu, Haibin Wang *, Guangfei Xu, Cun Chu

College of Mechanical and Electrical Engineering, Northeast Forestry University, Harbin, 150040, China

ARTICLE INFO

Keywords:
Blueberry harvesting machinery
Transmission clearance
Orthogonal test
MLSD modeling
Field test

ABSTRACT

Since China possesses the vast territory and a large blueberry planting area, blueberry harvesting with hand is laborious and time consuming. As the blueberry planting agronomy in China is different from other countries, it is pretty significant to develop blueberry harvesting machinery applicable to the domestic planting agronomy to achieve mechanized harvesting of blueberries. In blueberry harvesting operation, the harvesting system as the core component of the machine is the key technology of the harvesting machinery. The previous study found that: in terms of harvesting machinery, most of the literature has studied the dynamic characteristics, while few articles have been published to study the transmission clearance. But the clearance collision force generated by the transmission clearance of the harvesting system directly affected the output load moment and harvesting force of the machine developed by acting on the plant, and then affected the picking efficiency and the quality of picked fruit. Therefore, this paper focuses on the study of the transmission clearance of the blueberry harvesting machine. Firstly, the MLSD modeling method was applied to establish the transmission clearance model of the harvesting device, and the corresponding mechanical analysis of the transmission clearance was carried out. Secondly, after programming in MATLAB software and simulation in ADAMS software, the correctness of the transmission clearance model of the harvesting device was verified in different environments. The multi-body dynamics analysis software ADAMS was used for building the transmission clearance model of the harvesting device and perform mechanical simulation to analyze the clearance collision force and the output load moment of the harvesting device. Pro/E, ADAMS and ANSYS software were integrated to establish the flexible body of blueberry plant. Then the flexible body was combined with the mechanical model of harvesting device for rigid-flexible coupling simulation analysis to study the fruit harvesting force under different transmission clearances. Finally, the orthogonal method was used to conduct field test on blueberry harvesting to study the influence of the transmission clearance on the quality of picked fruit and picking efficiency of the machinery. Therefore, the best combination of the transmission clearance of the harvester was obtained as follows: cam clearance (the clearance joints of cam) was 0.25 mm, the slider clearance was 0.2 mm, left connecting rod clearance pair was 0.1 mm, right connecting rod clearance pair was 0.2 mm; the field picking test was conducted to obtain the machine's picking efficiency was 3.93 kg min^{-1}, the shedding rate of unripe fruit was 3.1 %, and the damage rate of picked fruit was 2.8 %. The research findings of this paper can offer referenced basis and theoretical support for berry harvesting machinery, and also can provide guidance for the design and improvement of other agricultural and forestry harvesting machinery.

* Corresponding author.
E-mail addresses: mm666mmm233@163.com (X. Lyu), whb_nefu@nefu.edu.cn (H. Wang).

https://doi.org/10.1016/j.heliyon.2024.e34740
Received 16 September 2023; Received in revised form 14 July 2024; Accepted 16 July 2024
Available online 17 July 2024

1. Introduction

Currently, blueberries on the market in China are mainly obtained by hand-picking, which forces farmers to seek new harvesting methods to improve picking efficiency due to the harvesting difficulties and low picking efficiency [1–3]. Foreign blueberry harvesting technology is well-developed and has been mechanized, while blueberry harvesting technology in China is still in the research stage [4–11]. After related research, it was found that in forest fruit harvesting operations based on the harvesting vibration mechanism, the transmission clearance of harvesting machinery generated cumulative error and affected the mechanical performance, reduced the system motion accuracy. Moreover, the transient impact generated by the transmission clearance exacerbated the friction wear between the components [12,13]. However, in order to achieve the predetermined motion trajectory, transmission clearance inevitably existed in the harvester. Therefore, how to set the value of the transmission clearance between the kinematic pair to ensure that the system can achieve the predetermined trajectory as required, decrease the cumulative error, reduce the friction loss of the components and maximize the machine performance becomes the core problem in the study of forest fruit harvesting machinery.

In terms of transmission clearance, the form of motion and modeling methods of transmission clearance have been studied by domestic and foreign scholars limitedly [14–39]. Bauchau and Rodriguez performed kinematic and dynamical analysis of the clearance joint of a flexible multibody system [23]. Ming and Tien have studied the transmission performance of linkage mechanisms with joint clearance and have used the concept of equivalent virtual link to simulate actual mechanism with joint clearance [24]. Etesami et al. studied the slider-crank mechanism with transmission clearance, and used Pareto bi-objective genetic algorithm to optimize the transmission angle and realize dynamic balance of the mechanism so as to solve the problems of noise and abrasion caused by the existence of the clearance between the mechanism joints, and to improve the transmission quality appropriately [25]. Several people have taken the planar 4-bar mechanism as the object of study and optimized its design in order to reduce the undesirable vibrations caused by the existence of clearances in the mechanism [26,27]. Ji et al. analyzed chaotic motion states of crank rocker mechanisms with joint clearance [28]. Hayasaka and Okamoto researched the influence of hinge clearance on the mechanized properties of hinged truss structure [29]. Folkman et al. analyzed the influence of kinematic clearance on the damping of hinged space structure [30]. Dubowsky and Freudenstein considered the elastic deformation of the contact surfaces of the kinematic pair components, established the system dynamics equation and proposed clearance motion models for 1D impact pair, 1D impact bar and 2D impact ring [31]. Dubowsky and Gardner decomposed the relative motion state of the mechanism kinematic pair into three stages of separation-collision-contact and studied the system kinematic pair [32]. Furuhash et al. applied the continuous clearance model to study the 4-bar linkage mechanism and quantified the transmission clearance collision forces [33,34]. Wang et al. established a nonlinear spring-damping model conforming to the contact boundary conditions to describe the contact-collision process of the system clearance, and obtained the dynamics equation of the linkage mechanism with clearance and studied them [35]. Xiao et al. studied the nonlinear dynamics problem of the mechanism with clearance and used the perturbation method to analyze the system clearance motion [36].

The above study analyzed the system transmission clearance motion form and modeling methods. Checking relevant literature obtained that, in the light of harvesting machinery, most of the literature have studied the dynamics characteristics and analyzed the interaction force between the agricultural machinery and the fruit, while few articles have been published to study the transmission clearance [40–43]. But the clearance collision force generated by the transmission clearance directly affected the machine harvesting system (the output load moment and blueberry fruit harvesting force), and then affected the picking efficiency and the quality of the picked fruit. In this paper, MLSD modeling method was applied to analyze the transmission clearance of blueberry harvesting machinery system and established the elastic-damping model of transmission without clearance. The mechanical analysis on the transmission clearance of the harvesting system was conducted to analyze the effect of the transmission clearance of the harvesting device on the related fruit harvesting force. Then, the testing research of the transmission clearance of the harvesting system on the picking efficiency and the quality of the picked fruit was implemented, which laid the theoretical grounding for the design of blueberry harvesting machinery and accelerated the mechanization process of domestic blueberry harvest. In addition, the research findings of this paper can offer referenced basis and theoretical support for berry harvesting machinery, and also can provide guidance for development and improvement of other agricultural and forestry harvesting machinery.

2. Materials and methods

2.1. Research overview

In this paper, domestic and foreign research findings were referred to study the transmission clearance of blueberry harvesting device. The Massless Rod-Spring-Damping model (MLSD model) transformed the mechanical structure into a dynamic model consisting of a massless rod (representing the clearance stiffness), a spring (representing the clearance elasticity), and a damper (representing the damping properties of the clearance), which made the model easy to understand and analyze. And the parameters can be adjusted to suit different clearance characteristics. Then the clearance model was established by using the MLSD method, and the kinematic and dynamics analysis were carried out to study the vibration response of blueberry plants after manual pruning under the action of the harvesting device. Finally, the clearance equation of the device and the blueberry plant vibration equation under the action of the blueberry harvesting machinery were obtained as shown in Table 1.

After consulting the literature, it is found that MATLAB software (MATLAB 9.5, R2018b, September 2018, MathWorks, U.S.) is a scientific calculation software, which has been used by a wide range of scholars to perform theoretical analysis in-depth in their

respective fields with good results. Since this software fits well with the research content of this paper, MATLAB software is used in this paper for mechanical analysis of the transmission clearance of the harvesting device.

In this paper, ADAMS software (ADAMS 2020, February 2020, Mechanical Dynamics Inc, U.S.) was used to research the clearance collision process under machine working conditions. The reason for this is that ADAMS software is a multi-body dynamics analysis software, which is mainly applied for analyzing the interaction forces between objects, and the software functions are in conjunction with the study content of this article, and the analysis results obtained from this software have certain reference value. Therefore, ADAMS software is used in this paper to study the clearance collision force of the transmission device of the harvesting machinery and the fruit harvesting force under the clearance collision force, and the simulation results under ADAMS software are compared and analyzed with that under MATLAB software. However, the use of the two aforementioned software inevitably will produce some deviations with the practical results when performing the simulation analysis, which is the boundedness of this research.

The flow chart of this paper is shown in Fig. 1. Firstly, working principle and machine structure of the blueberry harvesting machinery were analyzed, and the mechanical structure of the transmission clearance of the harvesting device was studied, then the corresponding mechanical model was established.

Secondly, the harvesting device transmission clearance model was simulated and analyzed in two different software programs, MATLAB and ADAMS, respectively. And the obtained collision force was compared with the transmission clearance parameters and values set in Table 2 and Table 3. The flexible body model (blueberry plant after manual pruning) was established by integrating Pro/E (WildFire 5.0, September 2009, Parametric Technology Corporation, U.S.), ANSYS (ANSYS Workbench 2019 R2, June 2019, ANSYS corporation, U.S.), ADAMS software and relevant mechanical parameters of the branch, and the rigid body model of the machine was established based on Table 4.

Thirdly, based on Equations (14)–(17), the rigid-flexible coupling connection settings were made for these two models, and the fruit harvesting force under the action of different clearances was analyzed in ADAMS software. Then the fruit harvesting force, picking efficiency and the quality of picked fruit under different clearances were researched through field picking test. Finally, the combination of transmission clearance of the harvesting device that can achieve the best picking efficiency was obtained comprehensively.

2.2. Analysis of the structure and the transmission clearance of the harvester

2.2.1. Working principle and structure of the harvester

The working principle diagram of the harvester was shown in Fig. 2, the harvester was mainly composed of components such as the gathering device of the plant, the walking system, the gantry frame, driven device of the harvesting system, the transmission device of the harvesting system and the end-execution elements (combs).

When the blueberry harvesting machine was taking the harvesting operation, the harvesting machine rid the ridge operation forward; the blueberry plant after manual pruning was gathered into the gantry frame of the machine through the gathering device; and the driven device of the harvesting system drove the combs on both sides to oscillate reciprocally left and right by the transmission device, then the blueberry plant passing the gantry frame was struck to form vibration to remove the fruit above the branches and realize the mechanical harvesting of blueberry.

Among them, the gantry frame was welded with angle iron; the combs were the end-execution elements of the harvesting system. The main role of the driven device of the harvesting system was to reduce the rotational speed of the driven elements and oscillating frequency of the combs, increase the output moment of the driven elements, change the direction of rotation. The main role of the transmission device was to change the form of movement of the driven device and convert the rotation motion of the driven elements into reciprocating oscillation of the combs of the harvester.

The structure diagram of the harvesting system of the harvester is shown in Fig. 3, which consists of three parts: drive device (composed of engine, mechanical continuously variable transmission, conveyor, worm reducer), transmission device (composed of groove cam, cam roller, push rod, linear bearing, guided block, push rod connector, slider roller, slider, rocker, connecting rod shaft,

Table 1
Summary table of theoretical equations related to the harvesting collision of blueberry fruit.

Sequence number	Description of the equation
1	Closing vector expression of transmission clearance function in the blueberry harvesting device
2	Expression for cam transmission device
3	Expression for the azimuth of the transmission clearance of the transmission pair on the push rod-left comb
4	Expression for the function of the clearance collision force on the cam transmission device
5	Expression for the function of the clearance collision force on the double-rocker transmission device
6	MLSD model function equation for the transmission clearance of the harvesting device
7	Moment equation for the rotational center of the grooved cam
8	Equation for the force analysis of the push rod
9	Equation for the equilibrant moment of combs on both sides
10	Equation for the force analysis of the connecting rod
11	Geometric model of blueberry plants
12	Mechanical model of blueberry plants under the action of comb torque
13	Expressions for the vibration output response of blueberry plants
14	Expression for blueberry fruit harvesting force
15	Expression for blueberry fruit harvesting conditions

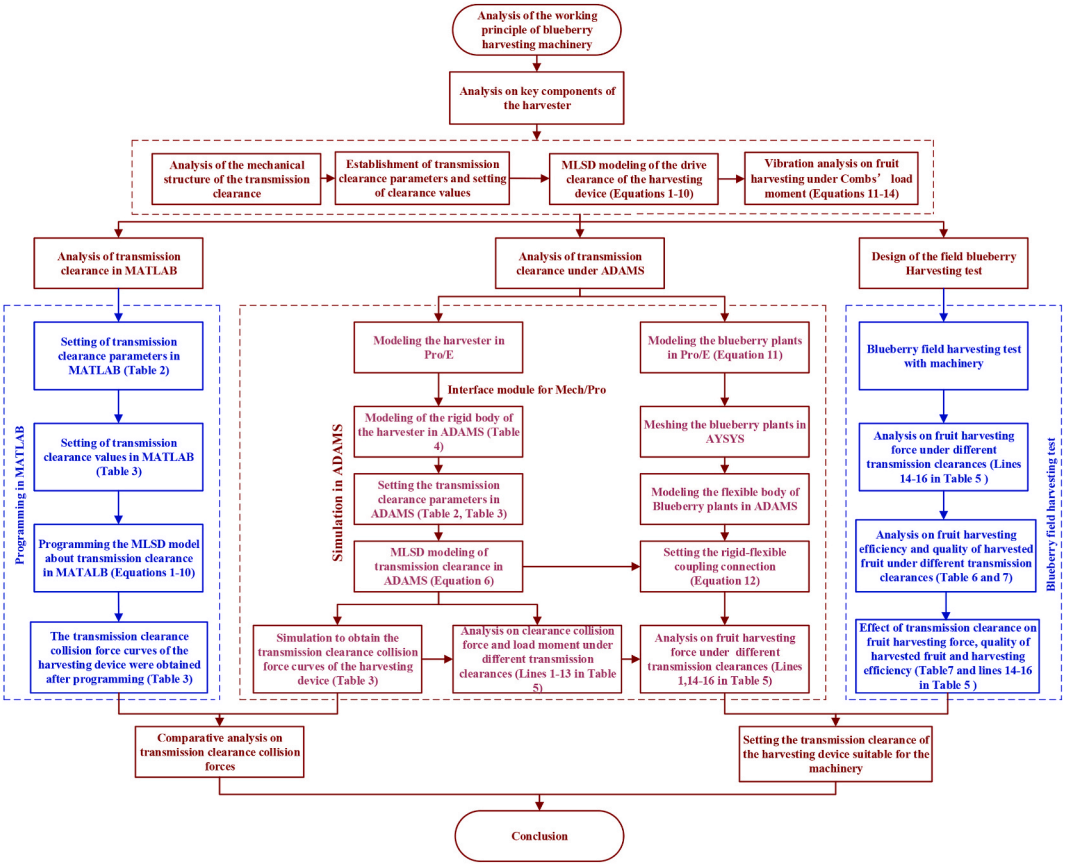

Fig. 1. Flow chart of the whole study.

connecting rod, combs' shaft) and combs.

The working principle of the specific harvesting system was shown below: engine, as the output impetus of the driven element of the harvesting system, adjusted the speed through the mechanical continuously variable transmission speed, and drove the worm reducer to rotate through the belt drive; the engine drove the groove cam to rotate, while changing the transmission direction to increase the output torque of the system, so that the cam roller slid along the cam groove at the same time to drive the push rod movement; the push rod drove the push rod connector and the slider roller in a linear reciprocating motion under the joint guidance of the linear bearing and guided block; slider roller reciprocated in the groove of the slider through the rocker and the connecting rod to drive the combs on both sides around the combs shaft, while doing reciprocating linear motion, and the blueberry plant passing the combs was struck to realize the fruit mechanical harvesting.

2.2.2. Analysis on key components of the harvester

After analyzing the structure diagram of the harvesting system (Fig. 3), the principle diagram of the harvesting system can be obtained, as shown in Fig. 4. The analysis of Fig. 4 shows that the harvesting system is mainly composed of a groove cam mechanism and a double-rocker mechanism.

In Fig. 4, the base circle radius of the cam is set as r_0, the stroke is set as h and the eccentricity is set as e. The cam rotates clockwise at an angular speed ω. According to the cam rise angle δ_0, far angle of repose δ_{01}, motion angle for return travel $\delta_0^{'}$ and near angle of repose δ_{02}, the displacement curve of the push rod can be divided into push stage, distal resting stage, return stage and near resting stage,. And the analysis diagram of the can transmission mechanism is obtained, which can be shown in Fig. 5. In Fig. 5, $s(\phi)$ is the motion curve of the cam mechanism that determines the motion law of the push rod; the cam curve. $s(\phi)$ includes polynomial curve and trigonometric function curve. Because the quintic polynomial curve has no rigid impact and flexible impact in the process of movement, and the NC milling process is easy to ensure the cam profile. Then, the quintic polynomial curve is adopted as the motion curve of the cam mechanism.

According to the start and stop boundary conditions of cam push and return stage as well as the cam design parameters, the six element-first order equation was established and the undetermined coefficients of the quintic polynomial curve of cam were solved. The motion curve of the cam mechanism $s(\phi)$ is obtained, which can be expressed as:

Table 2
Summary table of the parameters of the harvesting drive.

Sequence number	Parameter	Parameter name	Units	Numerical value	Reference	Note
1	m_2	Mass of push rod	(kg)	1.615		
2	m_3	Mass of the left comb	(kg)	8.384		
3	m_4	Mass of the connecting rod	(kg)	0.949		
4	m_5	Mass of the right comb	(kg)	8.066		
5	l_{AB}	Length of the push rod	(mm)	626		
6	$l_{B'D}$	Length of the rocker	(mm)	145		
7	l_{CD}	Length of the rocker of the left comb	(mm)	90		
8	l_{CF}	Length of the connecting rod	(mm)	310		
9	l_{FE}	Length of the rocker of the right comb	(mm)	90		
10	l_{DE}	Distance between the left and right side of the comb shaft	(mm)	340		
11	n_1	Rotational speed of the camshaft	(r min^{-1})	120		$\omega_1 = \frac{\pi n_1}{30}$
12	μ_2	Friction coefficient between push rod and linear bearing		0.05	44–46	
13	μ_3	Friction coefficient between combs and branch		0.05	44–46	
14	δ_1	Transmission clearance of cam pair	(mm)	0.5		
15	δ_2	Transmission clearance of slider pair	(mm)	0.3		
16	δ_3	Transmission clearance of left connecting rod clearance pair	(mm)	0.12		
17	δ_4	Transmission clearance of right connecting rod clearance pair	(mm)	0.12		
18	K_c	Equivalent stiffness coefficient	(N m^{-1})	5.75×10^6	44,45, 47–49	
19	C_c	Equivalent damping coefficient	(N s m^{-1})	0.175	44,45, 47–49	
20	l	Length of the blueberry branch	(m)	0.4		
21	d_0	Diameter of the root of the branch	(m)	1.5×10^{-2}		
22	d_m	Diameter of the end of the branch	(m)	0.8×10^{-2}		

Table 3
Transmission clearance value table of the harvesting device in MATLAB.

Sequence number	Transmission clearance of cam pair A/(mm)	Transmission clearance of slider pair B/(mm)	Transmission clearance of connecting rod pair C/(mm)	Transmission clearance of connecting rod pair F/(mm)
1	0.3	0	0	0
2	0	0.5	0	0
3	0	0	0.12	0
4	0	0	0	0.18

Table 4
Connection relationship of each component.

Sequence number	Name	Connecting Component 1	Connecting Component 2
1	Fixed pair	Gantry frame	Ground
2	Fixed pair	Driven elements	Gantry frame
3	Revolute pair	Groove cam	Driven elements
4	Point curve joint	Groove cam	Cam roller
5	Fixed pair	Cam roller	Push rod
6	Revolute pair	Push rod	Harvester frame
7	Fixed pair	Slider rod	Push rod
8	Point curve joint	Slider	Slider roller
9	Fixed pair	Left comb	Slider
10	Revolute pair	Gantry frame	Left comb
11	Revolute pair	Left comb	Connecting rod
12	Revolute pair	Connecting rod	Right comb
13	Revolute pair	Right comb	Gantry frame

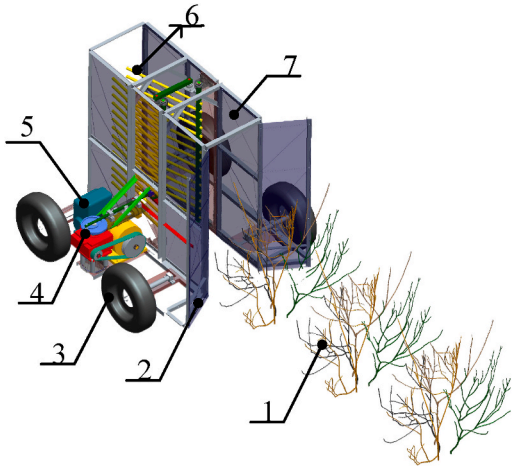

Fig. 2. The working principle diagram of the harvester. 1. Blueberry plant 2. Gathering device 3. Walking system 4. Harvesting device 5. Driven device 6. combs 7. Gantry frame.

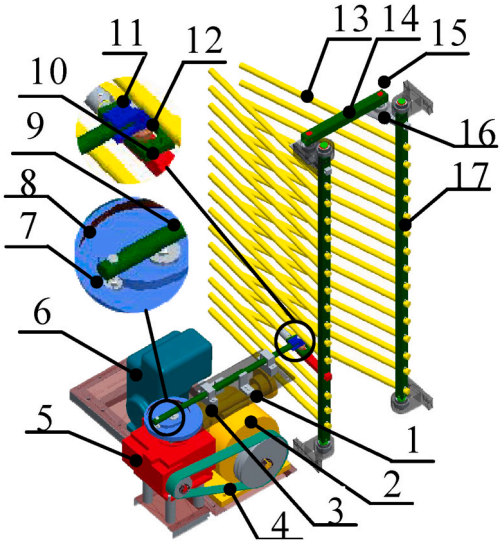

Fig. 3. The structure diagram of the harvesting system. 1. Guided block 2. Mechanical continuously variable transmission 3. Linear bearing 4. Conveyor 5. Worm reducer 6. Engine 7. Cam roller 8. Groove cam 9. Push rod 10. Slider 11. Push rod connector 12. Slider roller 13. combs 14. Connecting rod 15. Connecting rod shaft 16. Rocker 17. combs shaft.

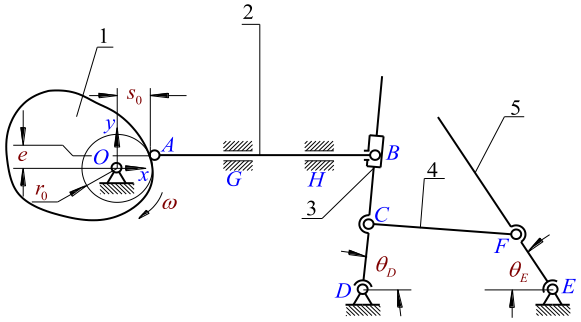

Fig. 4. The principle diagram of the harvesting system. 1. Groove cam 2. Push rod 3. Left comb 4. Connecting rod 5. Right comb.

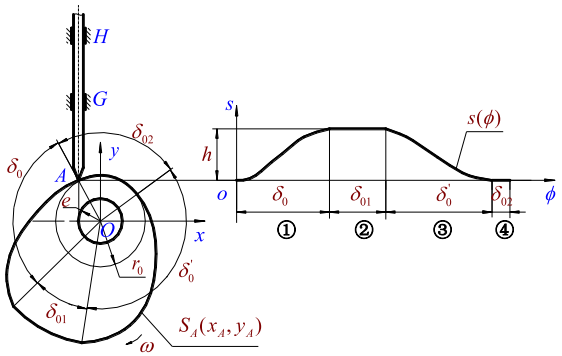

Fig. 5. Analysis diagram of the cam transmission mechanism.

$$s_A(\phi)=\begin{cases}\dfrac{10h}{\delta_0^3}\phi^3-\dfrac{15h}{\delta_0^4}\phi^4+\dfrac{6h}{\delta_0^5}\phi^5 & \phi\in\left(0,\delta_0\right]\\ h & \phi\in(\delta_0,(\delta_0+\delta_{01})]\\ \dfrac{10h}{\delta_0^3}(\psi-\phi)^3-\dfrac{15h}{\delta_0^4}(\psi-\phi)^4+\dfrac{6h}{\delta_0^5}(\psi-\phi)^5 & \phi\in\left((\delta_0+\delta_{01}),\left(\delta_0+\delta_{01}+\delta_0'\right)\right]\\ 0 & \phi\in\left(\left(\delta_0+\delta_{01}+\delta_0'\right),2\pi\right]\end{cases}\tag{1}$$

where, h is the can stroke (m); ϕ is the cam angle (rad); δ_0 is the cam rise angle (rad); δ_0' is the motion angle for return travel (rad); δ_{01} is the far angle of repose (rad); δ_{02} is the near angle of repose (rad); ψ is constant, the expression of which is: $\psi=2\pi+2\delta_0+\delta_{01}$ (rad); $s(\phi)$ is the displacement curve of the push rod angle (rad).

According to the curve motion curve of the cam mechanism $s(\phi)$, the groove cam profile curve can be expressed as:

$$\begin{cases}x(\phi)=[s_0+s_A(\phi)]\cdot\cos\phi-e\cdot\sin\phi+kr_r\dfrac{[s_0+s_A(\phi)]\cos\phi-e\sin\phi}{\sqrt{[s_0+s(t)]^2+e^2}}\\ y(\phi)=[s_0+s_A(\phi)]\cdot\sin\phi+e\cdot\cos\phi-kr_r\dfrac{[s_0+s_A(\phi)]\sin\phi+e\cos\phi}{\sqrt{[s_0+s_A(\phi)]^2+e^2}}\end{cases}\tag{2}$$

where, x is horizontal coordinate of the groove cam profile curve (m); y is longitudinal coordinate of the groove cam profile curve (m); e is the cam eccentricity distance (m); r_0 is the base circle radius of the cam (m); s_0 is the x-direction distance between the end of the push rod A and the cam center O, when the push rod is in the near rest stage, which can be expressed as: $s_0=\sqrt{r_0^2-e^2}$ (m); r_r is the cam roll radius, $r=0$ corresponds groove cam theoretical profile curve, (m); k is the factor of the groove cam profile curve, $k=-1$ corresponds groove cam inner profile curve, $k=-1$ corresponds groove cam outer profile curve, (m).

The double rocker transmission mechanism in Fig. 5 was analyzed. According to the established cam motion curve, it can be obtained that the swing Angle of the finger bank on both sides of the double rocker mechanism can be expressed as:

$$\begin{cases}\theta_D=\cot^{-1}\left[\dfrac{s(t)+l_{AB}+\sqrt{r_0^2-\left(y_B-y_O\right)^2}-x_D}{y_B-y_D}\right]\\ \theta_E=\cos^{-1}\dfrac{l_{DE}^2+l_{CE}^2-l_{DC}^2}{2l_{DE}l_{CE}}+\cos^{-1}\dfrac{l_{CD}^2+l_{CE}^2-l_{CF}^2}{2l_{CD}l_{CE}}\end{cases}\tag{3}$$

where, x is horizontal coordinate of the groove cam profile curve (m); y is longitudinal coordinate of the groove cam profile curve (m); θ_D is the rotation angle of the left comb around the rotation center D at any time t (rad); θ_E is the rotation angle of the right comb around the rotation center E at any time t (rad); $s(t)$ is the time displacement curve of the push rod, which can be expressed as: $s(t)=s_A(\omega t-2\pi n)$, and $n\in\{0,N^+\}$, $(\omega t-2\pi n)\in(0,2\pi]$ (m); y_B is the coordinate of the B of the push rod on the y-axis (m); y_O is the cam rotation center O on the y-axis (m); x_D is the coordinate of the rotation center of the left comb D on the x-axis (m); y_D is the coordinate of the rotation center of the left comb D on the y-axis (m); l_{CF} is the length of the connecting rod CF (m); l_{DE} is the distance between the two points D and E in the comb center on left and right sides (m); l_{DC} is the distance between the two points D and C in the left comb (m); l_{CE} is the distance between the point C in the connecting rod and the rotation center E in the right comb (m).

2.2.3. Analysis on the transmission clearance of the harvesting system

During the operation process of the fruit harvesting machinery, since the transmission clearance existed in each kinematic pair of

the harvesting device inevitably, and produced the corresponding clearance collision force, which affected the output torque and the harvesting collision force of the combs, then affected the picked fruit's quality and the picking efficiency (as shown in Fig. 6).

For this reason, this paper mainly analyzed the transmission clearance of the harvesting machinery and carried out picking test to study the influence of the collision force generated by the transmission clearance of the machine on the picked fruit's quality and picking efficiency.

The mechanical structure diagram of the transmission clearance of the harvester was shown in Fig. 7. From the figure, it can be obtained that there are four clearances that will cause the kinematic error of the transmission parts of the harvesting system and thus affect the kinematic and dynamic characteristics of the combs on both sides: the transmission clearance pair of groove cam I, the transmission clearance pair II between the push rod and the left comb, the transmission clearance pair III between the connecting rod and the hinge point of the left comb, the transmission clearance pair IV between the connecting rod and the hinge point of the right comb.

The mechanical structure of the clearance of the gearing system of the harvester is obtained by enlarging the mechanical structure of the four clearances in the partial view of Fig. 7, the analysis of which can be found that: when the harvester works, the cam roller rolls along the cam path of the groove cam, and it is concluded that both the groove cam and the cam roller are the main elements of the transmission clearance of the cam pair, which are abbreviated as the cam clearance pair *A*; the push rod is driven by the push rod connector to drive the push rod roller in the slider groove for reciprocating motion, and it is concluded that the push rod roller and the slider are the main elements that constitute the transmission clearance pair of the left comb of the push rod, which are abbreviated as the slider clearance pair *B*; the left comb pivots around the left comb shaft, and drives the connecting rod to move by the left rod bearing assembly at *C* in the left side of the left comb, thus it is concluded that the left rod shaft of the connecting rod is the main element that constitutes the transmission clearance of the left comb, which is abbreviated as the connecting rod clearance pair *C*; similarly, it is found that the connecting rod drives the right comb to pivot around the right comb shaft by the right rod bearing assembly at *F*, thus it is concluded that the right rod shaft is the main element that constitutes the transmission clearance of the connecting rod pair of the right comb, which is abbreviated as the connecting rod clearance pair *F*; since the cam clearance pair and slider clearance pair are both elements moving in the groove, they can be classified as point-line transmission clearance pair; the connecting rod clearance pair *C* and connecting rod clearance pair *F* are shaft bore transmission clearance matching, which can be classified as shaft bore transmission clearance pair. In other words, there are two main types (four pairs) of transmission clearance pair that affect the dynamic characteristics of the harvesting device.

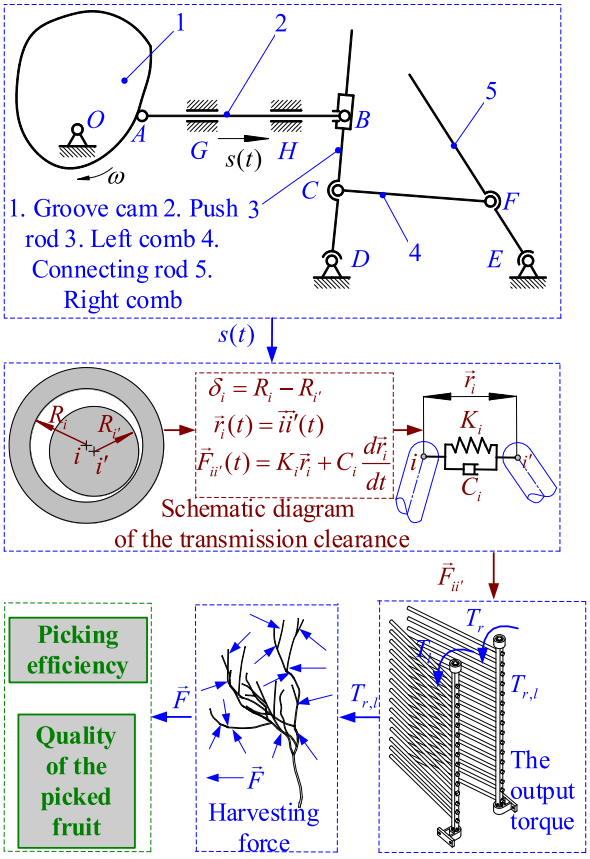

Fig. 6. Effect analysis diagram on the transmission clearance of the harvesting device.

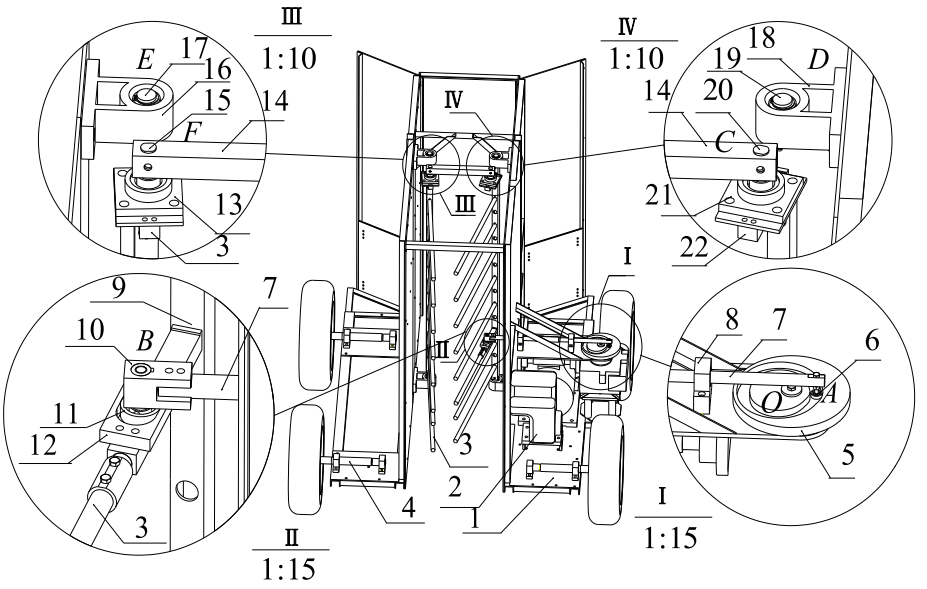

Fig. 7. Mechanical structure diagram on the transmission clearance of the harvesting device. 1. Gantry frame 2. Driven elements 3. Right comb 4. Walking system 5. Groove cam 6. Cam roller 7. Push rod 8. Linear bearing bracket 9. Left comb shaft 10. Push rod connector 11. Slider roller 12. Slider 13. Bearing assembly on right side of connecting rod 14. Connecting rod 15. Right side of connecting rod shaft 16. Right comb bearing bracket 17. Right comb shaft 18. Left comb shaft 19. Left comb shaft 20. Left side of connecting rod shaft 21. Bearing assembly on left side of connecting rod 22. Left comb.

2.3. Modeling on the transmission clearance of harvesting device

Since the transmission clearance of the above-mentioned kinematic pair in Fig. 7 was very small, the time of collision and separation between the transmission elements was extremely short. In order to reasonably carry out the analysis and simplify the calculation, the MLSD modeling and analysis method was used to obtain the kinematic model of the transmission clearance of the harvesting device as shown in Fig. 8. From this figure, the transmission clearance between each kinematic pair of the harvesting device was equated as a massless rod whose length varied with time.

Taking the cam rotation center as the origin of coordinates, a rectangular coordinate system was established, which was shown in Fig. 8. According to this figure, the transmission device constituted a closed vector from $''O \to A' \to A \to B' \to B \to D \to O''$, and a closed vector from $''D \to C' \to C \to F \to F' \to E \to D''$. The following closed vector equations were obtained by the "Complex Vector Method".

$$\begin{cases} l_{OA'}e^{j\theta_O} + r_A e^{j\beta_A} + l_{AB}e^{j\theta_{AB}} + r_B e^{j\beta_B} + l_{B'D}e^{j\theta_D} = 0 \\ l_{C'D}e^{j\theta_D} + r_C e^{j\beta_C} + l_{CF}e^{j\theta_{CF}} + r_F e^{j\beta_F} + l_{F'E}e^{j\theta_E} + l_{DE}e^{j\theta_{DE}} = 0 \end{cases} \tag{4}$$

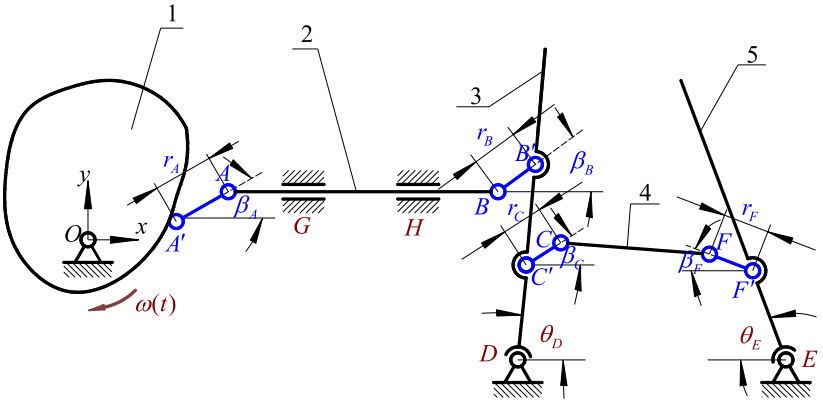

Fig. 8. Kinematic model on transmission clearance of harvesting device.

where, $l_{OA'}$ is the distance between the cam rotation center O and the collision point A' in the cam, which can be expressed as: $l_{OA'} = \sqrt{\left[s(t) + \sqrt{r_0^2 - (y_A - r_A \sin\beta_A - y_O)^2}\right]^2 + (y_A - r_A \sin\beta_A - y_O)^2}$ (m); l_{AB} is the distance between the point A and B in the push rod (m); $l_{B'D}$ is the distance between the rotation center D of the left comb and the collision point B' of the push rod (m); $l_{C'D}$ is the distance between the center of the left comb D and the collision point C' of the left comb (m); θ_O is the rotation angle of the cam around the rotation center (rad); θ_{AB} is the angle between the push rod AB and the X-Axis (rad); r_A is the transmission clearance of the cam pair (m); r_B is the transmission clearance of the slider pair (m); β_A is the azimuth of the transmission clearance r_A, in other words, the angle between the transmission clearance of the cam pair r_1 and the x-Axis (rad); β_B is the azimuth of the transmission clearance r_B, in other words, the angle between the transmission clearance of the slider pair r_B and the X-Axis (rad); $l_{C'D}$ is the distance between the left comb center D and the collision point C' in the left comb (m); l_{FE} is the distance between right comb center E and the collision point of the right comb F' (m); θ_4 is the angle between the connecting rod CF and the x-Axis (rad); θ_{DE} is the angle between the line connecting the comb center on left and right sides and the x-Axis (rad), $\theta_{DE} = 0$ (rad); r_3 is the transmission clearance at the hinge point of the connecting rod pair C (m); r_4 is the transmission clearance at the hinge point of the connecting rod pair F (m); β_3 is the azimuth of the transmission clearance r_3, in other words, the angle between the transmission clearance r_3 at the hinge point of the connecting rod pair C and the x-Axis (rad); β_4 is the azimuth of the transmission clearance r_4, in other words, the angle between the transmission clearance variable r_4 at the hinge point of the connecting rod pair F and the x-Axis (rad).

The expression for the azimuth of the transmission clearance of the push rod-left comb transmission pair β_B is as follows:

$$\beta_B = \beta_B^0 + \omega_B t + a_B t^2 \tag{5}$$

where, β_B^0 is the initial azimuth of the transmission clearance r_B, when $t = 0$, $\beta_B^0 = \beta_B|_{t=0}$ (rad); ω_B is the undetermined coefficient of the azimuth β_B of the transmission clearance r_B, $\omega_B \approx \dot{\beta}_B$ (rad s^{-1}); a_B is the undetermined coefficient of the azimuth β_B of the transmission clearance r_B, $a_B \approx 0$ (rad s^{-2}).

Due to the low harvesting frequency when the harvester was working, it was obtained that: $\ddot{r}_A \approx 0$ $\ddot{r}_A \approx 0$, $\ddot{r}_B \approx 0$, $\ddot{r}_C \approx 0$, $\ddot{r}_D \approx 0$, $a_B \approx 0$. A review of the relevant literature showed that the azimuth of the kinematic forces of the kinematic pair of the mechanism with clearance were approximately the same as those of the kinematic pair of the mechanism without clearance [50–52].

And Equation (4) were expanded to the two coordinate axes to solve the first-order derivative and second-order derivative. Equation (5) were substituted into the first-order derivative to obtain the kinematic characteristics of the cam transmission device and the double-rocker transmission device by simplification.

$$\begin{cases} \dot{s}(t) + \dot{r}_A \cos\beta_A^0 + \dot{r}_B \cos(\beta_B^0 + \omega_B t) - r_B\omega_B \sin(\beta_B^0 + \omega_B t) + l_{B'D}\dot{\theta}_D \cdot \sin\theta_D = 0 \\ l_{OA'}\omega_1 \cdot \cos\theta_O + \dot{r}_A \sin\beta_A^0 + \dot{r}_B \sin(\beta_B^0 + \omega_B t) + r_B\omega_B \cos(\beta_B^0 + \omega_B t) - l_{B'D}\dot{\theta}_D \cdot \cos\theta_D = 0 \\ \ddot{s}(t) - 2\dot{r}_B\omega_B \sin(\beta_B^0 + \omega_B t) - r_B\omega_B^2 \cos(\beta_B^0 + \omega_B t) + l_{B'D}\ddot{\theta}_D \cdot \sin\theta_D + l_{B'D}\dot{\theta}_D^2 \cdot \cos\theta_D = 0 \\ 2\dot{r}_B\omega_B \cos(\beta_B^0 + \omega_B t) - l_{O'A}\omega_1 \cdot \sin\theta_O - r_B\omega_B^2 \sin(\beta_B^0 + \omega_B t) - l_{B'D}\ddot{\theta}_D \cdot \cos\theta_D + l_{B'D}\dot{\theta}_D^2 \cdot \sin\theta_D = 0 \end{cases} \tag{6}$$

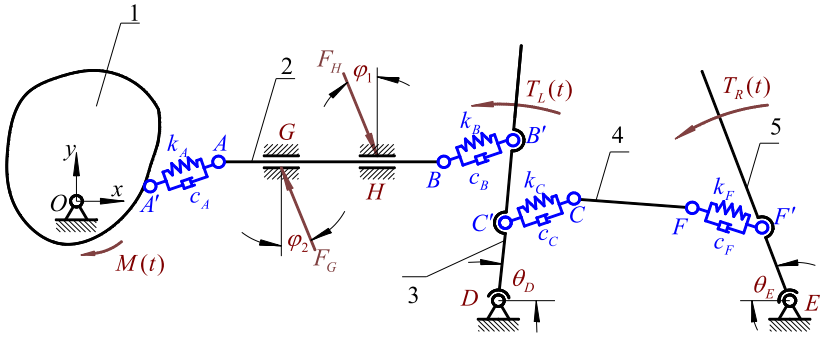

Fig. 9. Dynamics model of the transmission clearance of the harvesting device. 1. Groove cam 2. Push rod 3. Left comb 4. Connecting rod 5. Right comb.

$$\begin{cases} -l_{CD}\dot{\theta}_D \sin\theta_D + \dot{r}_C \cos\beta_C - l_{CF}\dot{\theta}_F \sin\theta_F + \dot{r}_F \cos\beta_F + l_{FE}\dot{\theta}_E \sin\theta_E = 0 \\ l_{CD}\dot{\theta}_D \cos\theta_D + \dot{r}_C \sin\beta_C + l_{CF}\dot{\theta}_F \sin\theta_F + \dot{r}_F \sin\beta_F + l_{FE}\dot{\theta}_E \cos\theta_E = 0 \\ l_{CD}\ddot{\theta}_D \sin\theta_D + l_{CD}\dot{\theta}_D^2 \cos\theta_D + l_{CF}\ddot{\theta}_F \sin\theta_F + l_{CF}\dot{\theta}_F^2 \cos\theta_F - l_{FE}\ddot{\theta}_E \sin\theta_E - l_{FE}\dot{\theta}_E^2 \cos\theta_E = 0 \\ \left[\begin{array}{c} l_{CD}\ddot{\theta}_D \cos\theta_D - l_{CD}\dot{\theta}_D^2 \cdot \sin\theta_D + l_{CF}\ddot{\theta}_F \cos\theta_F - l_{CF}\dot{\theta}_F^2 \cdot \sin\theta_F \\ +l_{FE}\ddot{\theta}_E \cos\theta_E - l_{FE}\dot{\theta}_E^2 \sin\theta_E \end{array} \right] = 0 \end{cases} \tag{7}$$

where, ω_O is the rotational speed of the cam (rad s^{-1}); $\dot{s}(t)$ is the velocity of the push rod at any time t (m s^{-1}); $\ddot{s}(t)$ is the acceleration of the push rod at any time t (m s^{-2}); θ_F is the angle between the connecting rod CF and x-Axis (rad).

In order to analyze the clearance collision force between each clearance pair, the transmission clearance dynamics model of the harvesting device was obtained according to Fig. 6 (Analysis diagram on the transmission clearance of the harvesting device) and MLSD modeling method as shown in Fig. 9.

From this figure, it can be found that the cam clearance pair A, slider clearance pair B, connecting rod clearance pair C and connecting rod clearance pair F are simplified to the combined spring-damping model, with the stiffness of the elastic element being K_i, and the damping coefficient being C_i. Thus, the forces acting on the transmission clearance can be expressed as:

$$\begin{cases} |F_{\vec{r}i}| = K_i \cdot r_i(t) + C_i \cdot \dot{r}_i(t) \\ \vec{F}_{\vec{r}i} = [\cos\beta_i(t)]\vec{x} + [\sin\beta_i(t)]\vec{y} \end{cases} \tag{8}$$

where, $F_{\vec{r}i}$ is the collision force vector of the transmission clearance of the kinematic pair (N); $\vec{F}_{\vec{r}i}$ is the collision force direction vector of the transmission clearance of the kinematic pair (N); $r_i(t)$ is the transmission clearance variable of the kinematic pair at any time t (m); $\beta_i(t)$ is the angle between the transmission clearance variable of the kinematic pair $r_i(t)$ and x-Axis at any time t (rad); K_i is the equivalent stiffness coefficient of the transmission clearance of the kinematic pair (N m^{-1}); C_i is the equivalent damping coefficient of the transmission clearance of the kinematic pair (N s m^{-1}); note: the subscript i in the equation above is the each kinematic pair, $i = A, B, C, F$.

To facilitate the analysis, the dynamical model of the transmission clearance of the harvesting device shown in Fig. 9 was decomposed into the dynamical model of the transmission clearance of the groove cam (shown in Fig. 10) and the dynamical model of the transmission clearance of the double-rocker (shown in Fig. 11).

As shown in Fig. 10, after analyzing the groove cam transmission clearance mechanical model with point O as the force analysis point, it can be obtained that:

$$\sum_{i=1}^{n} M_{iO} = F_{AA'} \cos\beta_A \cdot (y_A - r_A \sin\beta_A^0 - y_O) - M(t) - F_{AA'} \sin\beta_A \cdot \left[s(t) + \sqrt{r_0^2 - (y_A - r_A \sin\beta_A^0 - y_O)^2} \right] + J_O \cdot \ddot{\phi}_1(t) = 0 \tag{9}$$

where, M_{iO} is the moment of the active force i on the collision point O of the groove cam (N m); $F_{AA'}$ is the collision force of the cam clearance pair (N); $M(t)$ is the driven moment of the cam clearance pair (N m); J_O is the moment of inertia of the groove cam about point O, $J_O = 0.0176$ (kg m^2).

Taking the push rod as the object of study, the force analysis on the push rod can be obtained as follows:

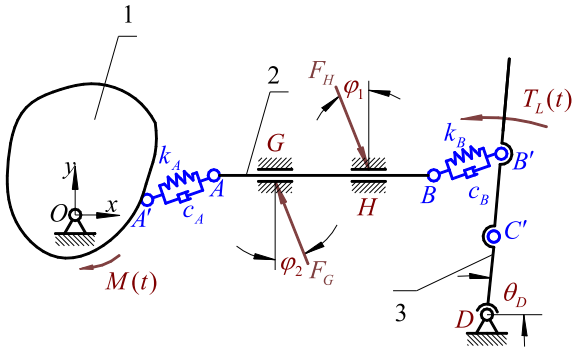

Fig. 10. Dynamical model of the transmission clearance of the groove cam. 1. Groove cam 2. Push rod 3. Left comb.

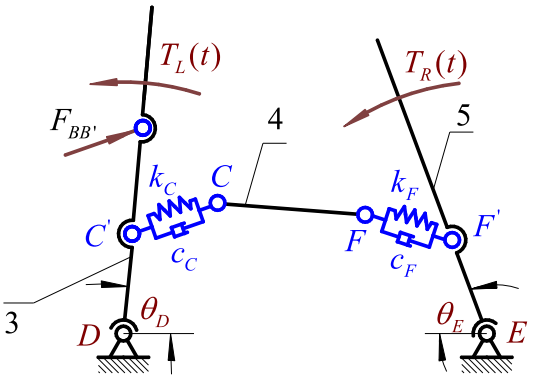

Fig. 11. Dynamical model of the transmission clearance of the double-rocker. 3. Left comb 4. Connecting rod 5. Right comb.

$$\begin{cases} \sum_{i=1}^{n} F_{ix} = F_{A'A}\cos\beta_A - F_G\sin\phi_2 - F_H\sin\phi_1 - F'_{BB'}\cos\beta_B = m_2\cdot\ddot{s}(t) \\ \sum_{i=1}^{n} F_{iy} = F_{A'A}\sin\beta_A + F_G\cos\phi_2 - F_H\cos\phi_1 - F'_{B'B}\sin\beta_B = 0 \\ \sum_{i=1}^{n} M_{iB} = \begin{bmatrix} -F_{A'A}\sin\beta_A\cdot l_{AB}\cdot\cos\theta_{AB} - F_G\cos\phi_2\cdot(l_{GH}+l_{HB})\cdot\cos\theta_{AB} + F_H\cos\phi_1\cdot l_{HB}\cdot\cos\theta_{AB} \\ +F_{A'A}\cdot\cos\beta_A\cdot\sin\theta_{AB}\cdot l_{AB} - F_G\cdot\sin\phi_2\cdot\sin\theta_{AB}(l_{GH}+l_{HB}) + F_H\cdot\sin\phi_1\cdot\sin\theta_{AB}\cdot l_{HB} \end{bmatrix} = 0 \end{cases} \tag{10}$$

where, M_{iB} is the moment of the active force i on the collision point B of the push rod (N m); $F_{BB'}$ is the clearance collision force of the slider pair (N); ϕ_2 is the friction angle between the push rod and the linear bearing, $\phi_2 = \arctan\mu_2$ (μ_2 is the corresponding friction coefficient between the push rod and the linear bearing)(rad); F_G is the force of the linear bearing on the push rod at the point G (N); F_H is the force of the linear bearing on the push rod at the point H (N); m_2 is the mass of the push rod (kg); l_{GH} is the length between the two points G and H on the push rod AB (m); l_{HB} is the length between the two points H and B on the push rod AB (m).

As shown in Fig. 11, for the double-rocker transmission mechanism: the torque of the left comb around point D is zero, and the torque of the right comb to point E is zero. Then it can be obtained:

$$\begin{cases} \sum_{i=1}^{n} M_{iD} = -F_{BB'}\sin(\theta_D-\beta_B)\cdot l_{B'D} + F_{CC'}\sin(\theta_D-\beta_C)\cdot l_{C'D} + \cos(\theta_D-\phi_3)\cdot T_l(t)|_{z=z_l} - m_3 l_3^2\cdot\ddot{\theta}_D + \frac{m_3 l_3^2}{3}\ddot{\theta}_D = 0 \\ \sum_{i=1}^{n} M_{iE} = F_{FF'}\cdot\cos(\beta_F-\theta_E)\cdot l_{F'E} + \sin(\theta_E-\phi_3)\cdot T_r(t)|_{z=z_r} + m_5 l_5^2\cdot\ddot{\theta}_E - \frac{m_5 l_5^2}{3}\ddot{\theta}_E = 0 \end{cases} \tag{11}$$

where, M_{iD} is the moment of the active force i on the collision point D of the left comb (N m); M_{iE} is the moment of the active force i on the collision point E of the right comb (N m); $\ddot{\theta}_D$ is the pendulum angular speed of the left comb (rad s^{-2}); $\ddot{\theta}_E$ is the pendulum angular speed of the left comb (rad s^{-2}); m_3 is the mass of the left comb (kg); m_5 is the mass of the right comb (kg); z_r is the position coordinate on the branch where the branch intersects with the right comb (m); z_l is the position coordinate on the branch where the branch intersects with the left comb (m); $T_l(t)$ is the load torque of the left comb $j \in \{r, l\}$ (N m); $T_r(t)$ is the load torque of the right comb $j \in \{r, l\}$ (N m); l_3 is the length of the left comb (m); l_5 is the length of the right comb (m).

Taking the connecting rod as the object of study, the force analysis on the connecting rod CF can be obtained as follows:

$$\begin{cases} \sum_{i=1}^{n} F_{ix} = F_{CC'}\cos\beta_C + F_{FF'}\cos\beta_F = m_4\cdot a_{4x} = 0 \\ \sum_{i=1}^{n} M_{iCF} = \begin{bmatrix} (F_{CC'}\cos\beta_C - F_{FF'}\cos\beta_F)\cdot\frac{l_4}{2}\sin\theta_4 + F_{CC'}\sin\beta_C\cdot\frac{l_4}{2}\cos\theta_4 \\ -F_{FF'}\sin\beta_F\cdot\frac{l_4}{2}\cos\theta_4 + \frac{m_4 l_4^2}{12}\ddot{\theta}_{CF} \end{bmatrix} = 0 \\ \sum_{i=1}^{n} F_{iy} = F_{CC'}\sin\beta_C + F_{FF'}\sin\beta_F = m_4\cdot a_{4y} = 0 \end{cases} \tag{12}$$

where, M_{iCF} is the moment of the active force i on the connecting rod CF (N m); $F_{CC'}$ is the transmission clearance collision force at the hinge point of the connecting rod pair C (N); $F_{FF'}$ is the transmission clearance collision force at the hinge point of the connecting rod

pair F (N); θ_4 is the angle between the connecting rod and the X-Axis (rad); a_{4x} is the acceleration component of connecting rod in the X-Axis direction (m s^{-2}); a_{4y} is the acceleration component of connecting rod in the Y-Axis direction (m s^{-2}); ϕ_3 is the friction angle between the left and right combs subjected to load force $P(t)$, $\phi_3 = \arctan \mu_3$ (μ_3 is the corresponding friction coefficient between the combs and blueberry plant)(rad); m_4 is the mass of the connecting rod (kg); l_4 is the length of the connecting rod (m).

Using θ_D, $\dot{\theta}_D$, $\ddot{\theta}_D$, r_A, $\dot{r}_A$, r_B, $\dot{r}_B$, ω_2, F_G and F_H as the unknowns, a one-dimensional unknown column vector X was obtained. To solve for the column vector X, Equations (5) and (6), (9) and (10) were combined and simplified to obtain the nonhomogeneous linear equation of the cam transmission device. The coefficient matrix of equations is a 10 × 10 non-singular square matrix.

Using θ_E, $\dot{\theta}_E$, $\ddot{\theta}_E$, θ_4, $\dot{\theta}_4$, $\ddot{\theta}_4$, r_C, $\dot{r}_C$, r_F, $\dot{r}_F$, $T_l(t)$ and $T_r(t)$ as the unknowns, a one-dimensional unknown column vector Y was obtained. To solve for the column vector Y, Equations ((5), (7), (11) and (12) were combined and simplified to obtain the nonhomogeneous linear equation of the double-rocker transmission device. The coefficient matrix of equations is a 11 × 11 non-singular square matrix.

Since both the cam transmission device and the double-rocker transmission device were the nonhomogeneous linear equations, the corresponding unknown column vectors X and Y were able to be solved. After solving for each transmission clearance of the harvesting device and the azimuth of each transmission clearance, the clearance collision force of each transmission pair and the load moment of the comb acting on the blueberry branch were calculated and obtained using Equation (8) and the MLSD model.

Based on the fact that the radius of a blueberry branch (from the root to the end) gradually changes decreasingly as the length of the branch increases, the variation coefficient of the cross-section of the blueberry branch α is obtained and expressed as:

$$\alpha = \frac{d_0 - d_m}{d_0} \tag{13}$$

where, α is the variation coefficient of the cross-section of the blueberry branch; d_0 is the diameter of the bottom position of the blueberry branch, $z = 0$ (m); d_m is the diameter of the end position of the blueberry branch, $z = l$ (m).

The length of the blueberry branch is assumed to be l, and the position of the blueberry branch is represented by the variable z. According to the Eulerian theory of material mechanics, the vibration equation of the blueberry branch under the action of the comb's load moment $T_l(t)$ and $T_r(t)$ can be expressed as:

$$\frac{\partial^2}{\partial^2 z}\left[EI(z)\frac{\partial^2 f(z,t)}{\partial^2 z}\right] + \rho A(z)\frac{\partial^2 f(z,t)}{\partial^2 t} = \frac{T_j(t)|_{z=z_j}}{l_j} \tag{14}$$

where, z is the coordinate of any section of the blueberry branch on the Z-Axis, $z \in [0, l]$ (m); $I(z)$ is the moment of inertia on the any section of the blueberry branch z (m^4); E is the elastic modulus of the plant (N m^{-1}); ρ is the density of the blueberry plant (kg m^{-3}); $A(z)$ is the sectional area of any section of the branch z (m^2); z_j is the position coordinate of the intersection between the branch and the comb on the branch, $j \in \{r, l\}$ (m); l_j is the position of the intersection between the branch and the comb on the comb, $j \in \{r, l\}$ (N m); $T_j(t)$ is the load torque of the left and right combs, $j \in \{r, l\}$ (N m).

Since Equation (14) is a partial differential equation, the Bessel function is used as the kernel function, and Equation (14) is solved by Duhamel integral. Then, the dominant mode, regular mode, vibration weight function, vibration output response and fruit harvesting force of the blueberry branch are obtained and can be expressed as:

$$\begin{cases} f^*(\varepsilon, t) = \sum_{k=1}^{r} F_k^*(\varepsilon) \cdot \Omega_k^*(t) \\ \Omega_k^*(t) = \dfrac{F_k^*\left(1 - \alpha\frac{z_j}{l}\right)}{\omega_{dk} l_j} \int_0^t T_j(\tau)|_{z=z_j} \cdot e^{-\xi\omega_{nk}(t-\tau)} \cdot \cos[\omega_{dk}(t-\tau)]d\tau \\ F_k^*(\varepsilon) = \dfrac{1}{a^2\sqrt{\int_1^{1-\alpha} \varepsilon^2 F_k^2(\varepsilon)d\varepsilon}} \cdot F_k(\varepsilon) \\ F_k(\varepsilon) = c_{1k}\dfrac{J_2\left(2a\sqrt{\omega_{dk}\varepsilon}\right)}{4a^2\omega_{dk}\varepsilon} + c_{2k}\dfrac{Y_2\left(2a\sqrt{\omega_{dk}\varepsilon}\right)}{4a^2\omega_{dk}\varepsilon} + c_{3k}\dfrac{I_2\left(2a\sqrt{\omega_{dk}\varepsilon}\right)}{4a^2\omega_{dk}\varepsilon} + c_{4k}\dfrac{K_2\left(2a\sqrt{\omega_{dk}\varepsilon}\right)}{4a^2\omega_{dk}\varepsilon} \end{cases} \tag{15}$$

where, ε is the position function of the blueberry branch, the expression of which is $\varepsilon = 1 - \alpha\frac{z}{l}$; a is the growth mechanical parameters of blueberry branches, the expression of which is $a = \frac{2l\rho^{\frac{1}{4}}}{\alpha E^{\frac{1}{4}} d_0^{\frac{1}{2}}}$ (s$^{1/2}$ m$^{-3/4}$); ξ is the damping ratio of the blueberry plant due to structural damping; ω_{nk} is the undamped intrinsic frequency of the blueberry plant (rad^{-1}); ω_{dk} is the damped intrinsic frequency of the blueberry plant (rad^{-1}); $F_k(\varepsilon)$ is the dominant mode of the blueberry branch (m); $F_k^*(\varepsilon)$ is the regular mode of the blueberry branch (m); $\Omega_k^*(t)$ is the regular vibration weight function; $J_2\left(2a\sqrt{\omega_{dk}\varepsilon}\right)$ is the second order first kind Bessel function; $Y_2\left(2a\sqrt{\omega_{dk}\varepsilon}\right)$ is the second order second kind Bessel function; $I_2\left(2a\sqrt{\omega_{dk}\varepsilon}\right)$ is the second order deformation first kind Bessel function; $K_2\left(2a\sqrt{\omega_{dk}\varepsilon}\right)$ is the second order deformation second kind Bessel function; c_{ik} $(i = 1, 2, 3, 4)$ is the dominant mode coefficient corresponding to the k order intrinsic frequency of the blueberry branch, which is determined by the boundary conditions.

According to the above results, under the flapping action of the comb, the vibration harvesting force of blueberry fruit growing on the blueberry branch z_m $F(\varepsilon_m, t)$ can be expressed as:

$$F(\varepsilon_m, t) = m_0 \cdot \frac{\partial^2 [f^*(\varepsilon, t)]}{\partial t^2}\Big|_{\varepsilon=\varepsilon_m, z=z_m} \tag{16}$$

where, z_m is the coordinate of where the blueberry fruit grows (m); ε_m is the position function corresponding to the growth position of the blueberry fruit $z_m z_m$ (m); m_0 is the mass of the blueberry fruit that grows on the branches z_m (kg); $F(\varepsilon_m, t)$ is the fruit harvesting force (N). During the operation process of the harvesting machinery, the machine is required to pick the ripe fruit and retain the unripe one at the same time. Then the harvesting condition of the harvesting device meeting the target of the machine can be expressed as:

$$F_a \leq F(\varepsilon_m, t) \leq F_b \tag{17}$$

where, F_a is the bonding force between the ripe fruit and the blueberry branch, $F_a = 0.26 \sim 0.3$ N[47,48]; F_b is the bonding force between the unripe fruit and the blueberry branch, $F_b = 1.0 \sim 3.6$ N[47,48].

2.4. Simulation setup of transmission clearance model of harvesting device in MATLAB

Based on the structure diagram of the harvesting system shown in Fig. 3, the material of each component of the harvesting transmission device was set to steel, and the material of the end-execution elements (combs) was set to nylon, so that the dimensional parameters, mass parameters and working parameters of each kinematic part of the harvesting transmission device were obtained. After consulting the relevant references, the equivalent stiffness coefficient and equivalent damping coefficient of each transmission clearance pair of the harvesting device were set, and the summary of parameters was obtained, as shown in Tables 2 [46–49,53,54].

According to the mechanical structure of the harvesting transmission device, the transmission clearance values of each kinematic pair were set in MATLAB software. And the transmission clearance value table of the harvesting device was obtained as shown in Table 3.

2.5. Simulation setup of transmission clearance model of harvesting device in ADAMS

Based on the working principle of the blueberry harvester (as shown in Fig. 2), Pro/E software was used to design the structure and components of the machine. The components were imported into the multi-body dynamics analysis software ADAMS through Mech/pro module. According to the harvesting system structure (as shown in Fig. 3), the connection relationship of each component of harvesting device was set as shown in Table 4.

In the environment of ADAMS, the material of each component of the harvesting transmission device was set to steel and the material of combs was set to nylon. To analyze the effect of the transmission clearance on clearance collision force of the transmission pair, the cam roller, slider roller and the connecting rod on both sides of the rotating shaft were parameterized so that the size of the transmission clearance of the harvesting device was able to be adjusted. The transmission clearance values of the harvesting device under ADAMS were shown in Table 5. After setting the transmission clearance values of cam clearance pair *A*, slider clearance pair *B*, connecting rod clearance pair *C* and connecting rod clearance pair *F*, the data in lines 1 to 13 in Table 5 were obtained. In order to analyze the influence of different transmission clearance on the load moment of the harvesting device, the clearance values of each transmission pair were set and the data in lines 14–16 in Table 5 were obtained.

Based on the connection relationship of the various components of the harvester in Table 4, the dimension parameters, mechanical parameters and the clearance values of each transmission pair of the harvesting transmission device model were set by referring to the parameters in Table 2 and Equation (8), and the mechanical model of the transmission clearance of the harvester was obtained, as shown in Fig. 12. In order to establish the flexible body (blueberry plant), the blueberry plant model was established in Pro/E software

Table 5
Transmission clearance value table of the picking device.

Sequence number	Transmission clearance of cam pair *A*/(mm)	Transmission clearance of slider pair *B*/(mm)	Transmission clearance of connecting rod pair *C*/(mm)	Transmission clearance of connecting rod pair *F*/(mm)
1	0	0	0	0
2	0.25	0	0	0
3	0.5	0	0	0
4	1.0	0	0	0
5	0	0.2	0	0
6	0	0.4	0	0
7	0	0.6	0	0
8	0	0	0.1	0
9	0	0	0.15	0
10	0	0	0.2	0
11	0	0	0	0.1
12	0	0	0	0.15
13	0	0	0	0.2
14	0.25	0.2	0.1	0.1
15	0.5	0.4	0.15	0.15
16	1.0	0.6	0.2	0.2

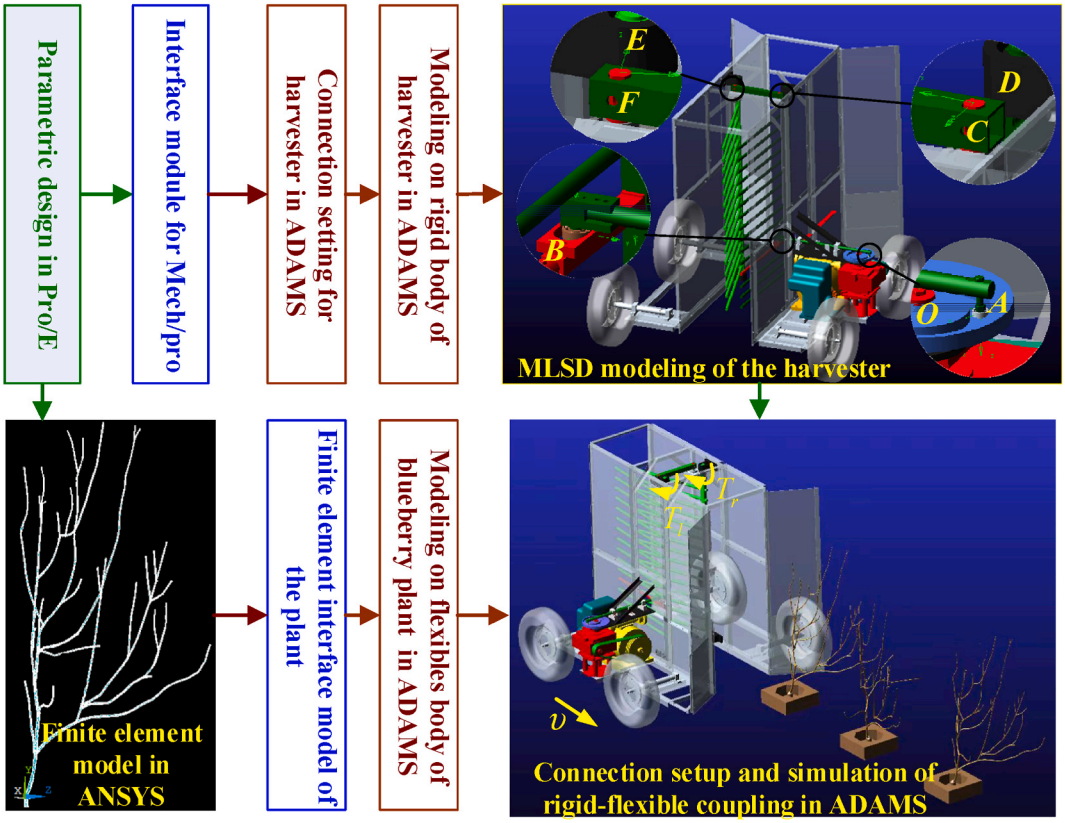

Fig. 12. Transmission clearance model of the harvesting device in ADAMS.

based on Equation (13) and the plant's growth parameters, which was imported into ANSYS software. Then, the root of the blueberry branch was set as the fixed end, and the end of the branch was set as the free end, according to the growth of the plant. The flexible body unit type was set as Solid Hex, the cross section of the branch was set as Elliptical. Blueberry plant mechanics parameters were set according to the parameters numbered 1–4 in Table 6.

Then, after meshing the plant model, the corresponding finite element model of blueberry plant was gained and the corresponding " *.mnf " file was generated. The generated blueberry plant flexible body file was transferred to ADAMS software to obtain the final flexible body model (blueberry plant). Based on Equations (15) and (16), the connection between the root of the plant and the ground was set as a fixed pair, and the "impact function method" was selected to calculate the interaction force between the harvester and the blueberry plant. According to the picking collision theory [11] of the interaction between the picker and the blueberry plant, the rigid-flexible coupling connection between the plant model and the transmission clearance model was set, including the setting of mechanical parameters (E_2, μ_2, ρ_2 and ξ) and contact parameters (μ_1, ρ_1, E_1, d_{max}, e and q). Parameter values are shown in Table 6. The walking speed of the machine was set to 30 m min^{-1}, and the interaction model between the rigid body (picking machinery) and the

Table 6
Setting parameter table of rigid-flexible coupling between blueberry plant and harvester.

Sequence number	Parameter	Parameter name	Unit	Parameter name	Literature resources	Notes
1	E_2	Elasticity modulus of branch	(MPa)	690	55	
2	μ_2	Poisson's ratio of branch		0.3	3	
3	ρ_2	Density of branch	(kg/m^3)	0.9×10^3		Measured in the test
4	ξ	Damping ratio of branch		0.1	50	
5	m_0	Fruit mass	(g)	1		Measured in the test
6	ρ_1	Density of the combs	Kg/m^3	1.15×10^3		Measured in the test
7	E_1	Elasticity modulus of the combs	(MPa)	30×10^3	55	
8	μ_1	Poisson's ratio of the combs		0.25	54	
9	d_{max}	Maximum penetration depth at collision point	(mm)	0.05	52, 53	
10	e	Collision recovery coefficient		1	52, 53	
11	q	Power exponent		1.5	11	

flexible body (blueberry plant) with transmission clearance was obtained, as shown in Fig. 12.

2.6. Design of picking field test

In order to analyze the consequence of the transmission clearance of the harvesting device on the harvesting effect of the machine so as to obtain the optimal transmission clearance of each kinematic pair, the study on picking test was conducted using the self-developed blueberry harvester (Northeast Forestry University, Harbin, Heilongjiang, China) (as shown in Fig. 13). The test was conducted in mid-July 2022 at the product R&D center of Taizhou Gang Yang Co., Ltd. in Jiangsu Province, China.

The field test was conducted in laboratory. The test subjects (blueberry variety) were "Bluecrop"; height of the tree was 1.5–1.7 m and tree-age was 7 years old (Although we carried out blueberry picking test with this variety of blueberries, the picking machine is not only suitable for picking blueberries of the " Bluecrop " variety. The machine is also suitable for highbush blueberries with the height of 0.8m–1.8 m). The artificially planted blueberry plant was transplanted to the middle position of the combs of the harvester, and the spacing of blueberry plants was set as 1.5 m, which was consistent with the spacing of blueberry plant in the field. A plastic film was placed under the blueberry plant to collect the fruit that was vibrated by the machine, during the picking test process. Since the collision force of the clearance between each kinematic pair was difficult to be measured, the picked fruit ‘s quality and picking efficiency of the harvester were used as the test indexes to assess the working performance of the harvesting system under different transmission clearances of each kinematic pair of the machine.

In the field picking test, cam roller, push rod roller and connecting rod of different sizes were replaced to set the transmission clearance value of each kinematic pair. The influence of four test factors (cam clearance *A*, slider clearance *B*, connecting rod clearance pair *C* and connecting rod clearance pair *F*) on the picked fruit’s quality and picking efficiency of the harvester was studied by using the orthogonal test method, in which three levels were set for each factor correspond to lines 14–16 in Table 5. Thus, a four-factor, three-level orthogonal table $L_9(3^4)$ was used as the test program.

3. Results and discussion

3.1. Analysis on transmission clearance collision force of harvesting device in different simulation environments

3.1.1. Analysis on transmission clearance collision force in MATLAB

By referring to the parameter setting of the simulation model in Table 2 in Section 2.3 and the transmission clearance values in Table 3, MATLAB software was used to program and calculate the transmission clearance model of the harvesting device according to Equations (4)–(11), and then the collision force curves of the clearance of each kinematic pair are shown in Figs. 14–17.

According to the analysis of Figs. 14–17, the maximum clearance collision force of cam transmission pair is similar to that of slider pair; and the mean value of clearance collision force of cam transmission pair is greater than that of slider pair; the maximum clearance collision force values of the left and right hinged points of the connecting rod pair are similar, and the mean clearance collision force of the left hinged point is greater than that of the right hinge point.

3.1.2. Analysis on transmission clearance collision force in ADAMS

In order to compare and analyze the transmission clearance model of the harvester in different software environments, the harvesting transmission device was set according to the connection relationship in Table 4, and the size parameters and mechanical parameters of the harvester were set in ADAMS in accordance with the data in Table 2 in MATLAB software. The clearance of each

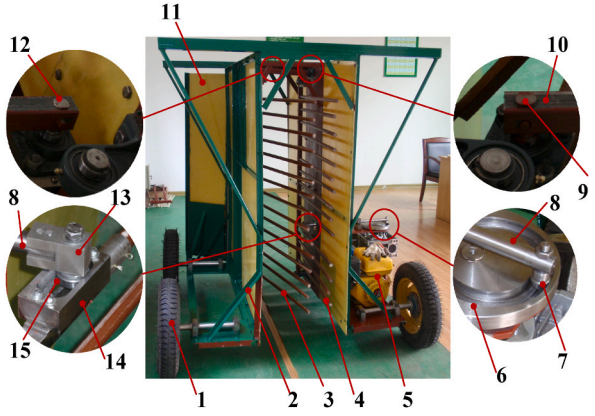

Fig. 13. Blueberry harvesting machinery. 1. Walking system 2. Gantry frame 3. Right comb 4. Left comb 5. Driven elements 6. Groove cam 7. Cam roller 8. Push rod 9. Left side of connecting rod shaft 10. Connecting rod 11. Gathering device 12. Right side of connecting rod shaft 13. Push rod connecter 14. Slider 15. Push rod roller.

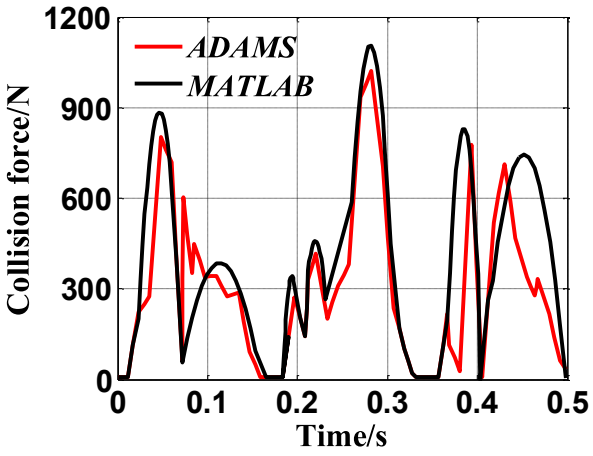

Fig. 14. Transmission clearance collision force curves of cam pair *A* (data in line 1, Table 3).

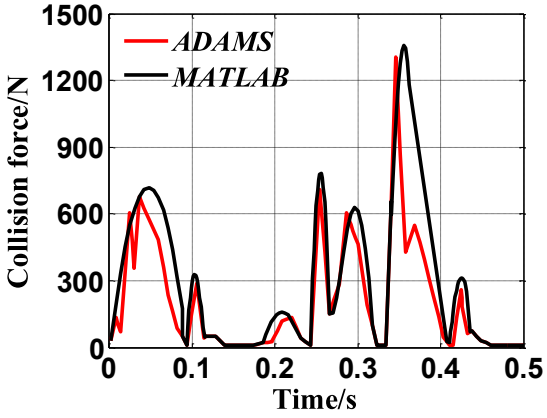

Fig. 15. Transmission clearance collision force curves of slider pair (data in line 2, Table 3).

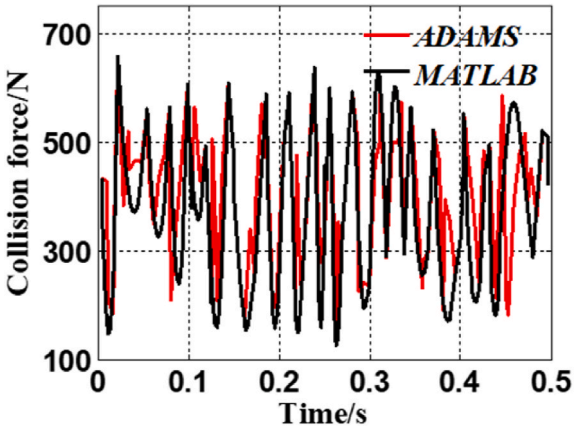

Fig. 16. Transmission clearance collision force curves of connecting rod pair (data in line 3, Table 3).

transmission pair was set with reference to the data in Table 3. After the dynamic simulation of the harvesting transmission device in ADAMS environment, the clearance collision force curves of each kinematic pair of the harvesting device were obtained, as shown in Figs. 14–17.

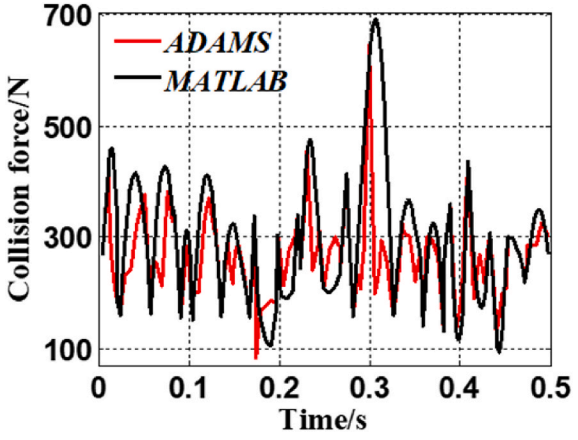

Fig. 17. Transmission clearance collision force curves of connecting rod pair (data in line 4, Table 3).

After analyzing the simulation curves shown in Figs. 14–17, the following conclusions are shown as follows: the overall variation tendency of the simulation curves in ADAMS is consistent with that in MATLAB; the value of clearance collision force obtained by simulation analysis is similar to the programming curves in MATLAB; there are some differences between programming curves in MATLAB and simulation curves in ADAMS in details, which is related to integration step and integration accuracy set by ADAMS software simulation. Taking the data points of curves in ADAMS and curves in MATLAB shown in Figs. 14–17 as the research objects, *F*-test method was used to calculate the correlation between curves in ADAMS and curves in MATLAB. The equation of *F*-test method is as follows:

$$F_{xy}=\frac{\sum_{i=1}^{m}(a_i-\overline{a})^2}{\sum_{j=1}^{n}\left(b_j-\overline{b}\right]^2}\frac{b_{\max}^2}{a_{\max}^2} \tag{18}$$

where, a_i and b_j are data points to be detected; $\overline{a}$ and $\overline{b}$ are the mean of the data points to be detected, $a_{\max}=\max\{a_i\}$, $b_{\max}=\max\{b_j\}$; F_{xy} is the *F*-test for data point a_i and data point b_j.

The test values of cures in ADAMS and MATLAB in Figs. 14–17 are respectively 2.3153, 2.5109, 2.1335 and 4.6904, which are smaller than the corresponding standard values of 3.20, 3.15, 3.089 and 3.092. There is no significant difference between the curves, indicating that: The curves in MATLAB programmed by equations (4)–(11) and ADAMS simulation curves with the same parameter Settings have a high degree of correlation and good fitting. It is concluded that the MLSD modeling and analysis method introduced in section 2.3 is suitable for the transmission clearance kinematics model of the picking device and can analyze the transmission clearance movement process of the picking device.

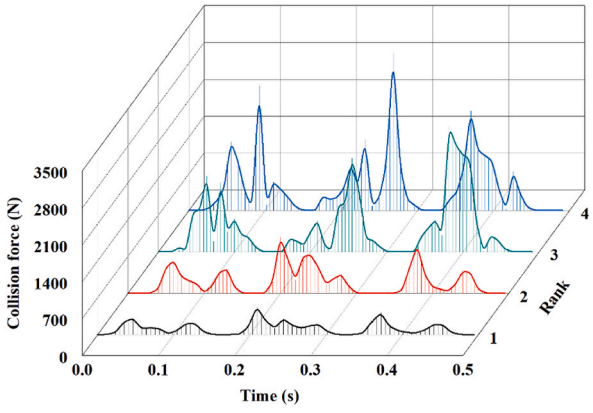

Fig. 18. Analysis of the effect of clearance collision force of cam pair *A*.

3.2. Analysis on clearance collision force of harvesting device under different clearances

In order to research the consequence of transmission clearance on the collision force of transmission pair, the dynamics simulation analysis on the established transmission clearance model of the harvesting device was carried out by using the single factor method and referring to the data in lines 1 to 13 in Table 5. The clearance collision force curves of each kinematic pair under different transmission clearance were obtained, as shown in Figs. 18–21 (Note: The Rank value in Figs. 18–21 corresponds to the data row number in Table 5, indicating the clearance collision force of the harvesting device in this setting of data.).

Comparing the curves from Figs. 18–21, it can be obtained that the clearance collision force of each kinematic pair is as follows: the clearance collision force of cam pair $A >$ the clearance collision force of slider pair $B >$ the clearance collision force of the connecting rod pair $C >$ the clearance collision force of the connecting rod pair F. The reason is that the cam pair A is located in front of the transmission chain of the harvesting device, the cam not only does the transmission movement and uses the power to drive the harvesting system to work, but also drives the movement of other parts of the harvesting device.

Therefore, the clearance collision force of the cam kinematic pair A is the largest. And with the continuation of the transmission chain, the kinematic parts driven by other kinematic pairs are gradually reduced, resulting in a gradual decrease in the clearance collision force. The final transmission pair of the transmission chain (connecting rod pair F) only drives the right comb to achieve reciprocating oscillation. Thus, the clearance collision force of the connecting rod pair F is the smallest. That is to say, the transmission collision force of each kinematic pair is related to the position of the transmission chain, and the transmission collision force of the kinematic pair located in front of the transmission chain is large, while the transmission collision force of the kinematic pair located behind the transmission chain is small.

Comparing the transmission curves without clearance (Rank 1) and the transmission curves with the clearance (other curves) in Figs. 18–21, the interaction force of each kinematic pair in the transmission without clearance is obviously smaller than that of each kinematic pair in the transmission with clearance, which is due to the existence of the transmission clearance. There is a certain kinematic space between each kinematic pair. When the harvester is working, each kinematic pair moves at a certain velocity and acceleration, and the existence of the transmission clearance makes each kinematic pair form extra velocity and acceleration after random motion in the kinematic space, which increases the clearance collision force.

Comparing the transmission curves with clearance in Figs. 18–21, it can be obtained that: with the increase of the transmission clearance, the mutual kinematic space of each kinematic pair increases, and the value of random velocity and random acceleration generated by random kinematic increase. Thus, the value of random collision force also increases. Due to the existence of transmission clearance and clearance collision force, the friction wear between each component increases, accelerating the wear of the machine, which affects the swing angle and output force of the combs (end-execution elements of the harvesting system) and affects the working performance of the harvesting system of the harvesting machine. It is thus obtained that, under the premise of ensuring smooth motion of the harvesting system, the smaller the transmission clearance, the better, while paying attention to the friction between the kinematic pair. In other words, due to the existence of the transmission clearance, the clearance collision force of each kinematic pair increases significantly, and the larger the transmission clearance, the greater the interaction clearance collision force of each kinematic pair.

3.3. Analysis on load moment of harvesting device under different clearances

When the blueberry harvester was in operation, the output load moment of the combs affected the fruit picking efficiency and the picked fruit's quality. In order to research the effect of transmission clearance on the load moment of both combs, the transmission clearance of each kinematic pair of the blueberry harvester was set separately by referring to the data in line 1, lines 14–16 in Table 5. Then the analysis diagram of the influence of load moment on both combs were obtained as shown in Figs. 22–23 (Note: the rank values in Figs. 22–23 corresponding to the sequence number in Table 5, which represent the load moment of the combs of the harvesting device under this setting of data.).

After analyzing Figs. 22 and 23, the output load moment on the left comb is larger than that on the right comb, the reason of which

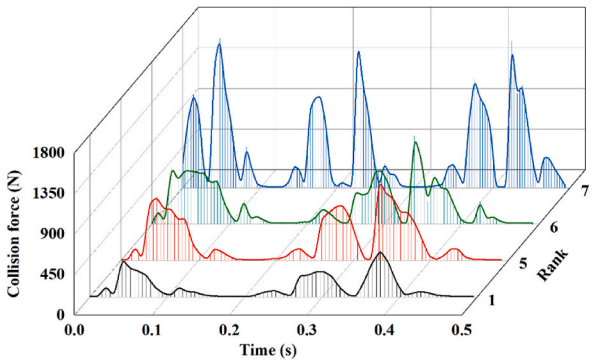

Fig. 19. Analysis of the effect of clearance collision force of slider pair B.

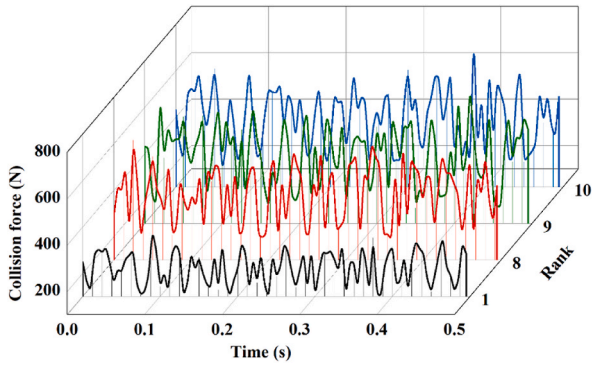

Fig. 20. Analysis of the effect of clearance collision force of connecting rod pair *C*.

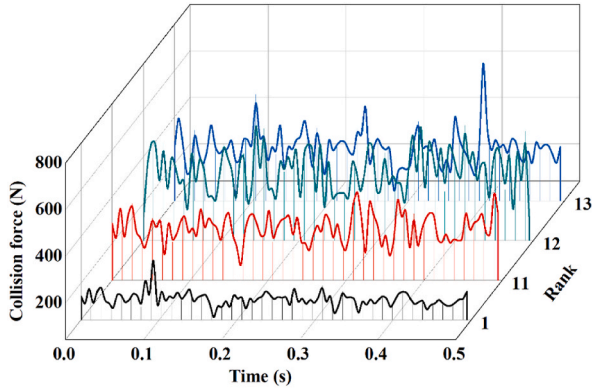

Fig. 21. Analysis of the effect of clearance collision force of connecting rod pair *F*.

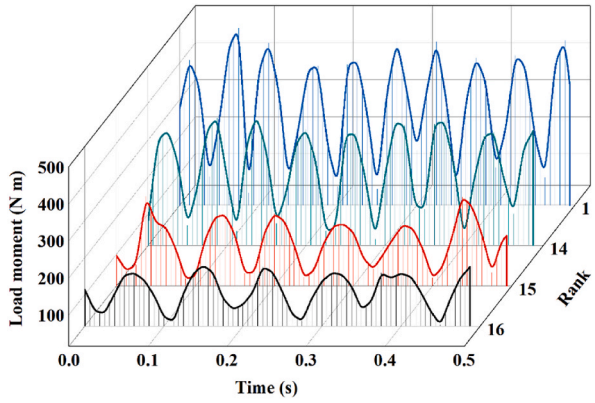

Fig. 22. Analytical diagram of the effect of load moment on the left comb.

is that the left comb is at the front of the transmission chain compared to the right comb. Comparing Figs. 22 and 23, the load moment of the combs without clearance transmission is larger than that with the clearance transmission; as the clearance increases, the output load moment of the combs decreases.

The reasons are as follows: when the harvester works, the combs on both sides run at a certain velocity and acceleration; since the combs have a certain mass, a certain load moment is needed to drive the combs for operation; there are transmission clearance in the cam pair *A*, slider pair *B*, connecting rod pair *C* and connecting rod pair *F*, which produce transmission error and error accumulation, and the larger the transmission clearance, the larger the error accumulation, and the larger the clearance collision force generated by the kinematic components, thus increasing the friction and damping force between the kinematic pair, consuming system energy and increasing the power dissipation of the system. Under the condition that the input power is certain, the increase of the power dissi-

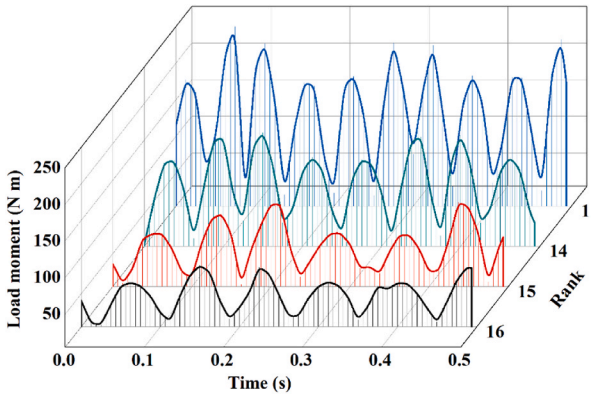

Fig. 23. Analytical diagram of the effect of load moment on the right comb.

pation reduces the output load moment of the combs.

In other words: the load moment of the transmission without clearance is greater than that of the transmission with clearance, and the larger the clearance, the greater the power dissipation of the system and the lower the output load moment of the combs.

3.4. Analysis of fruit harvesting force under different clearances

In order to study the consequence of the transmission clearance on the fruit harvesting force, the transmission clearance of each kinematic pair was set with reference to the data in the line 1, lines 14–16 of Table 5, respectively; and the kinetic simulation analysis of the established interaction model between the rigid body (the harvesting machinery) and the flexible body (blueberry plant) was

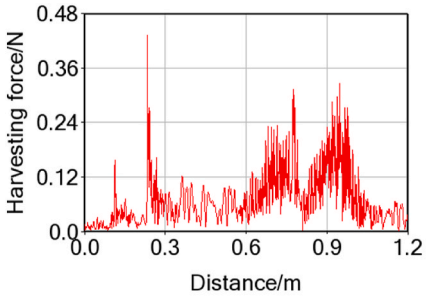

(a) Fruit harvesting force curves without transmission clearance

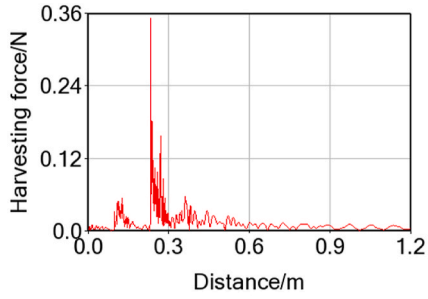

(b) Fruit harvesting force curves with small transmission clearance

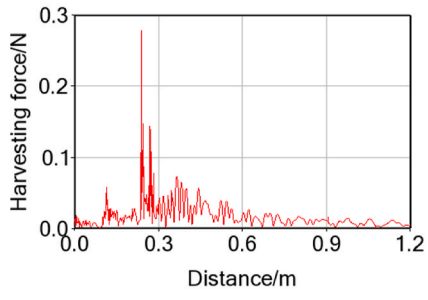

(c) Fruit harvesting force curves with medium transmission clearance

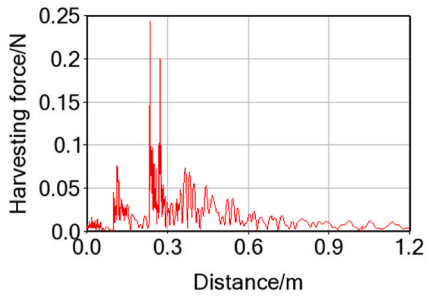

(d) Fruit harvesting force curves with large transmission clearance

Fig. 24. Blueberry fruit harvesting force curves at the root of the branch under different transmission clearances of the harvesting device. Note: Figures (a)–(b) correspond to the transmission clearance values in lines 1 and 14–16 of Table 5, respectively.

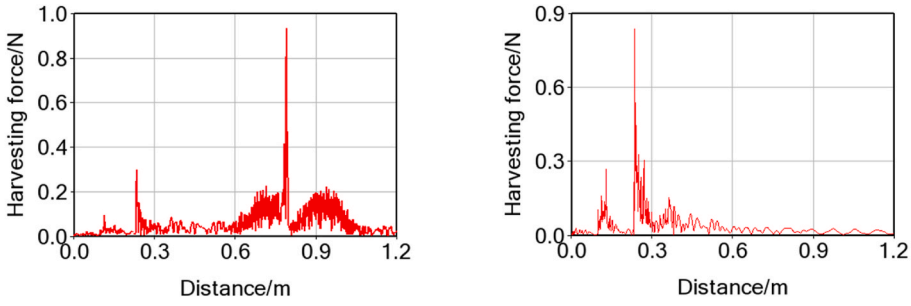

(a) Fruit harvesting force curves without transmission clearance

(b) Fruit harvesting force curves with small transmission clearance

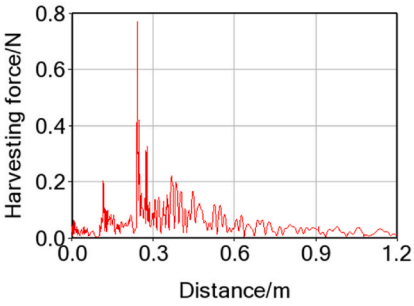

(c) Fruit harvesting force curves with medium transmission clearance

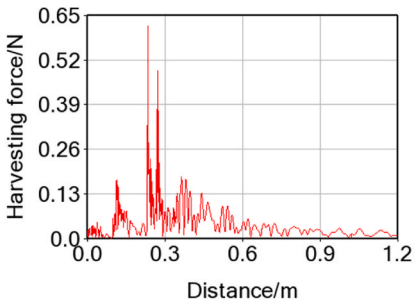

(d) Fruit harvesting force curves with large transmission clearance

Fig. 25. Blueberry fruit harvesting force curves at the middle of the branch under different transmission clearances of the harvesting device. Note: Figures (a)–(b) correspond to the transmission clearance values in lines 1 and 14–16 of Table 5, respectively.

carried out. Based on the above operation, the measurement curves about fruit harvesting force at different growth positions of blueberry branches with different transmission clearance as shown in Figs. 24–26.

In Figs. 24–26, the horizontal coordinates of the measurement curves are the distance between the running machine (the harvesting machinery) and the plant when interaction is generated, and the vertical coordinates are the corresponding blueberry fruit harvesting forces. Among them, Figs. 24–26 show the fruit harvesting forces on blueberry fruit growing at the root of the blueberry branch, growing in the middle of the blueberry branch and growing at the end of the blueberry branch under the action of the load moment of the harvester's combs, respectively.

Comparing the trends of the peak harvesting force curves from (a)–(d) in Figs. 24–26, the following conclusions can be drawn: with the increase of the collision clearance, the blueberry fruit harvesting force gradually decreases, which is due to the fact that the output load moment of combs in the harvesting machinery gradually decreases with the increase of the collision clearance; thus, the interaction force between the harvesting machine and the blueberry plant decreases, and the fruit harvesting force also gradually decreases. And with the change of blueberry fruit growth position (from the root to the end), the fruit harvesting force also gradually increases, which is due to the fact that under the action of the same load moment of the comb, the vibration output response of the blueberry branch gradually increases from the root to the end, and the vibration output response speed and acceleration also gradually increases. According to Equations (13)–(17), it can be obtained that with the change of blueberry fruit growth position, the fruit harvesting force gradually increases from the root to the end; the vibration output response gradually increases from the root to the end.

After analyzing the fruit harvesting force values from (a)–(d) in Figs. 24–26, it can be concluded that under the different combinations of transmission clearance, the fruit harvesting force ranges from 0.4 N to 0.25 N at the root of the blueberry branch; the fruit harvesting force ranges from 0.65 N to 0.9 N at the middle of the blueberry branch; the fruit harvesting force ranges from 0.8 N to 1.2 N at the end of the blueberry branch.

The bonding forces between the ripe fruit and branches F_a ranged from 0.26 N to 0.3 N, and the bonding forces between unripe fruit and branch F_b ranged from 1.0 N to 3.6 N. Based on the above findings and the distribution of fruit harvesting forces in the simulation curves, the following results can be drawn: under different combinations of transmission clearance, a few ripe fruit were not picked by the machine at the root of the blueberry branch; the harvesting quality was best in the middle of the blueberry branch (in other words, the ripe fruit was harvested, while the unripe fruit remained on the branch); the fruit harvesting force was greatest at the end of the blueberry branch, where not only all the ripe fruit was picked, but also a few unripe fruit was picked by the machine.

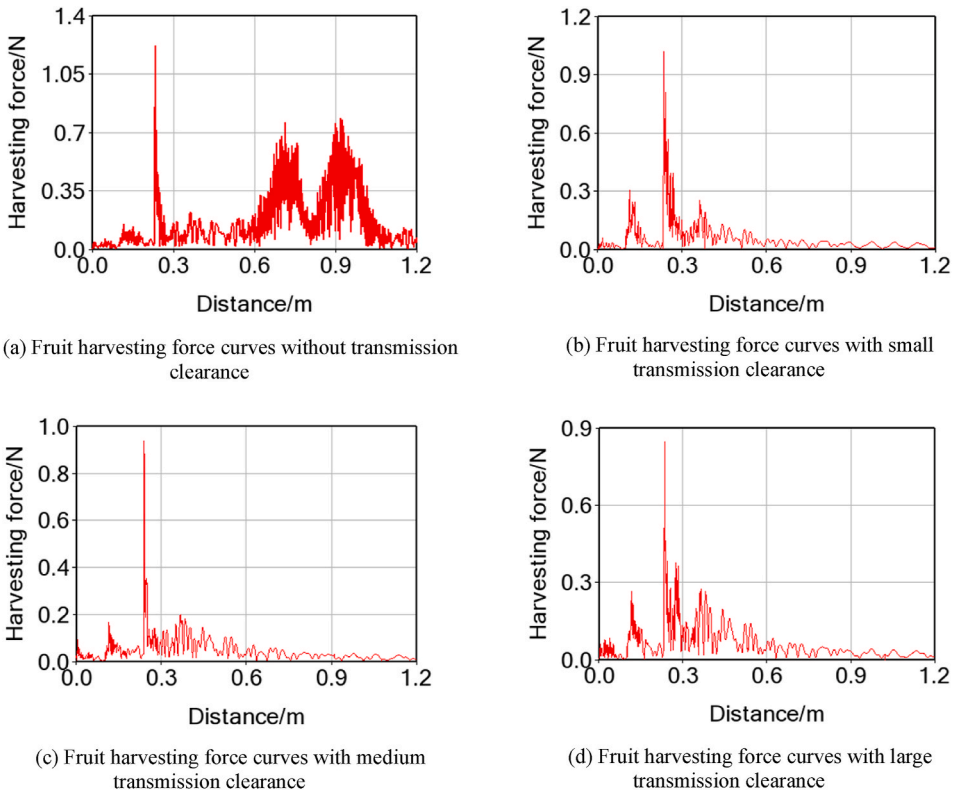

(a) Fruit harvesting force curves without transmission clearance

(b) Fruit harvesting force curves with small transmission clearance

(c) Fruit harvesting force curves with medium transmission clearance

(d) Fruit harvesting force curves with large transmission clearance

Fig. 26. Blueberry fruit harvesting force curves at the end of the branch under different transmission clearances of the harvesting device. Note: Figures (a)–(b) correspond to the transmission clearance values in lines 1 and 14–16 of Table 5, respectively.

3.5. Results and analysis of the field test

3.5.1. Picking results of the field test

In the field test, the harvesting walking speed was set to 30 m min^{-1}, the cam shaft rational speed of the harvester was set to 120 r min^{-1}, and the time of each picking test was set to 10 s. In the field test, it was found that there were a few unripe fruits remained at the root of the blueberry branch after picked, and a few unripe fruits at the end of the branch were vibrated off, and some unripe fruits remained in the harvested blueberry fruits. The reason for the above conclusion was as follows: when the coactions between the combs of the machine and blueberry plant occurred, the blueberry fruit harvesting force at the root of the blueberry branch was small, while the force at the end of the branch was large. Thus, there was a small amount of blueberry fruit at the root of the branch, and some unripe fruits at the end were vibrated off and retained in the harvested fruits, which was consistent with the simulation analysis results in section 3.4.

After the test, in order to study the results of the field picking test, the number of unripe fruit and the number of damaged fruit were counted from the picked fruit, and the quality of picked ripe fruit was measured by using precision electronic scales. The test indexes were defined as follows: the mass of picked fruit by the machine per minute was defined as the machine picking efficiency; the

Table 7
Statistical data of blueberry picking.

Sequence number	Cam clearance pair *A*/(mm)	Slider clearance pair *B*/(mm)	Connecting rod clearance pair *C*/(mm)	Connecting rod clearance pair *F*/(mm)	Picking efficiency/(kg m^{-1})	Shedding rate of unripe fruit/(%)	Damaged fruit rate/(%)
1	0.25	0.2	0.1	0.1	3.9	8.4	5.1
2	0.25	0.4	0.15	0.15	3.86	7.6	4.6
3	0.25	0.6	0.2	0.2	3.84	5.4	4.1
4	0.5	0.2	0.15	0.2	3.85	5.8	4.5
5	0.5	0.4	0.2	0.1	3.83	5.2	3.5
6	0.5	0.6	0.1	0.15	3.82	4.2	3.2
7	1.0	0.2	0.2	0.15	3.78	3.4	2.9
8	1.0	0.4	0.1	0.2	3.79	3.6	3.1
9	1.0	0.6	0.15	0.1	3.71	3.2	2.9

percentage of the mass of unripe fruit among the picked fruit to the mass of total picked fruit was defined as the rate of unripe fruit; the percentage of the mass of fruit damaged by picking to the mass of picked fruit was defined as the damage rate of picked fruit. The raw data obtained from the picking test were processed according to the above definitions to obtain the statistical data of picking test as shown in Table 7.

Comparison analysis of the 1st, 4th and 7th groups of test data in Tables 6 and it can be obtained that, with the increase of the collision clearance of the harvesting device, the picking efficiency of the harvester gradually decreases, the shedding rate of unripe fruit and damaged fruit rate gradually decrease. This is due to the fact that as the collision clearance increases, the load moment on the combs of the harvesting device gradually decreases, and the interaction force between the harvesting machinery and the plant gradually decreases; then the blueberry fruit harvesting force gradually decreases, the number of picked blueberry fruit gradually decreases, the number of unripe fruit shed and the number of damaged fruit decrease, which is consistent with the simulation analysis consequences in section 3.4. The transmission clearance of the picking device was set as the independent variable $x_i \quad (i = 1 \sim 4)$, and the picking efficiency, shedding rate of unripe fruit and damaged fruit rate are set as the dependent variable $y_i \quad (i = 1 \sim 3)$. The regression relationship between the dependent variable $y_i \quad (i = 1 \sim 3)$ and the independent variable $x_i \quad (i = 1 \sim 4)$ of the picking test was established by using the least squares method:

$$y_i = \begin{pmatrix} a_{i0} + a_{i1}x_1 + a_{i2}x_2 + a_{i3}x_3 + a_{i4}x_4 + c_{i1}x_1^2 + c_{i2}x_2^2 + c_{i3}x_3^2 + c_{i4}x_4^2 \\ +b_{i1}x_1x_2 + b_{i2}x_1x_3 + b_{i3}x_1x_4 + b_{i4}x_2x_3 + b_{i5}x_2x_4 + b_{i6}x_3x_4 \end{pmatrix} \tag{19}$$

where, $x_i \quad (i = 1 \sim 4)$ is independent variable corresponding to the clearance of the transmission pair of the picking device (mm); $y_i \quad (i = 1 \sim 3)$ is independent variable corresponding to the picking efficiency of the machine, shedding rate of unripe fruit and damaged fruit rate (mm); $a_{ij} \quad (j = 1 \sim 4)$ is the linear regression coefficient; $b_{ij} \quad (j = 1 \sim 6)$ is the cross-correlation regression coefficient; $c_{ij} \quad (j = 1 \sim 4)$ is the autocorrelation regression coefficient.

According to the test data in Table 7, the regression equation parameters in equation (19) were obtained by using DPS software, and the regression surface of the influence of transmission clearance of the picking device on the picked fruit quality and picking efficiency of the machine was obtained by MATLAB programming, as shown in Figs. 27–29.

Analysis of Figs. 27–29 (a) shows that: With the increase of the movement clearance of the slider pair, the picking efficiency of the machine increases at first and then decreases. The reason is that the vibration picking effect is presented by the composition between the swing frequency of the combs on both sides of the machine and the clearance value of the different slider clearance pair. When the swing frequency of the combs, the frequency response of the machine picking system and the natural frequency of the blueberry plant match, the picking vibration of the blueberry plant is near the resonance peak, resulting in the highest picking efficiency of the machine when the slide clearance pair is 0.4 mm. With the increase of the transmission clearance of the cam clearance pair, the clearance force gradually increases. Under the action of the clearance force, the motion hysteresis of the transmission element affects the output torque of the end executive element of the picking device, which reduces the fruit picking force and the picking efficiency of the machine.

As shown in Figs. 27–29 (b), as the transmission clearance of connecting rod pairs increases, the clearance collision force keeps increasing, the output torque of the combs decreases, the fruit picking force decreases, and the picking efficiency of the machine gradually decreases. This is the same as the simulation results obtained in Section 3.2, that is, as the clearance of the transmission pair

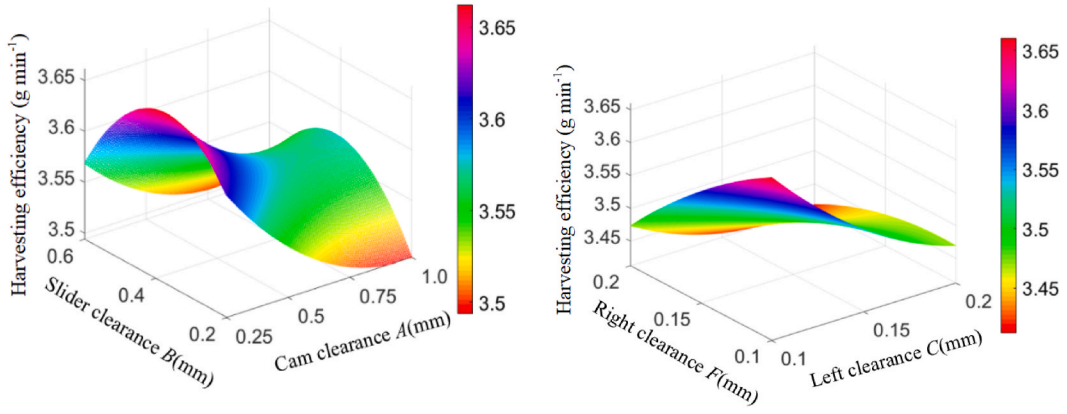

(a) Regression surface under the interaction influence between cam clearance pair A and slider clearance pair B

(b) Regression surface under the interaction influence between the connecting rod clearance pairs C and F

Fig. 27. Linear regression surface of picking efficiency.

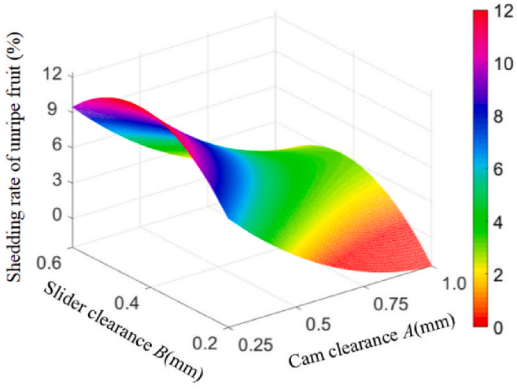

(a) Regression surface under the interaction influence between cam clearance pair A and slider clearance pair B

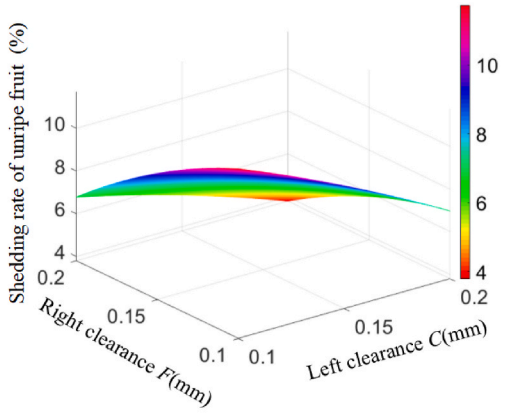

(b) Regression surface under the interaction influence between connecting rod clearance pairs C and F

Fig. 28. Linear regression surface of the shedding rate of unripe fruit.

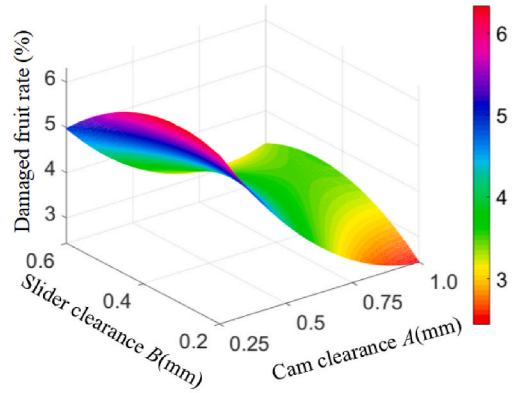

(a) Regression surface under the interaction influence between cam clearance pair A and slider clearance pair B

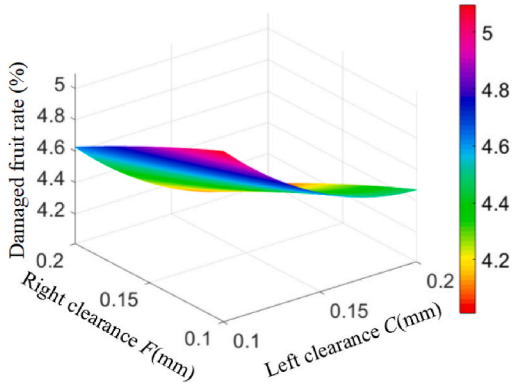

(b) Regression surface under the interaction influence between connecting rod clearance pairs C and F

Fig. 29. Linear regression surface of the damaged fruit rate.

increases, the clearance force increases, the output torque of the combs decreases, and the blueberry fruit picking force decreases under the composition between the picking device and the blueberry plant.

By analyzing the test data in Table 6, (a)-(b)in Figs. 27–29 and Equation (19) the values of various coefficients in the expression of dependent variable $y_i \quad (i = 1 \sim 3)$ corresponding to the picked fruit quality and picking efficiency were compared and analyzed: the conclusion can be obtained: The interaction of transmission clearance of the picking device does have certain effects on the picking efficiency and picked fruit quality (shedding rate of unripe fruit and damaged fruit rate), but the effects are very small. This is because the above four clearances only affect the performance of different structures of the picking system (groove cam mechanism, roller-slide reciprocating linear motion mechanism, left rocker swing mechanism and right rocker swing mechanism). And there is a certain independence between the mechanisms, the interaction between which is small and can be ignored. Therefore, the influence of interaction among test factors is not considered in the design and study of blueberry picking orthogonal test, as shown in Table 8.

3.5.2. Analysis of the field test results

According to the test data in Table 7, the orthogonal test table for blueberry picking was calculated, as shown in Table 8.

Table 8
Orthogonal test analysis table for blueberry picking.

Sequence number		Cam clearance A /(mm)	Slider clearance B /(mm)	Left clearance C /(mm)	Right clearance F /(mm)	Picking efficiency Y_1 /(kg m^{-1})	Shedding rate of unripe fruit Y_2 /(%)	Damaged fruit rate Y_3 /(%)
1		0.25	0.20	0.10	0.10	3.9	8.4	5.1
2		0.25	0.40	0.15	0.15	3.86	7.6	4.6
3		0.25	0.60	0.20	0.20	3.84	5.4	4.1
4		0.50	0.20	0.15	0.20	3.85	5.8	4.5
5		0.50	0.40	0.20	0.10	3.83	5.2	3.5
6		0.50	0.60	0.10	0.15	3.82	4.2	3.2
7		1	0.20	0.20	0.15	3.78	3.4	2.9
8		1	0.40	0.10	0.20	3.79	3.6	3.1
9		1	0.60	0.15	0.10	3.71	3.2	2.9
Picking efficiency	$\overline{K}_{11}$	11.6	11.53	11.51	11.44			
	$\overline{K}_{21}$	11.5	11.48	11.42	11.46	$\overline{T}_1 = 3.82$		
	$\overline{K}_{31}$	11.28	11.37	11.45	11.48			
	R_1	0.11	0.05	0.03	0.01			
Shedding rate of unripe fruit	$\overline{K}_{12}$	21.4	17.6	16.2	16.8			
	$\overline{K}_{22}$	15.2	16.4	16.6	15.2	$\overline{T}_2 = 5.20$		
	$\overline{K}_{32}$	10.2	12.8	14	14.8			
	R_2	3.73	1.6	0.73	0.67			
Fruit damage rate	$\overline{K}_{13}$	13.8	12.5	11.4	11.5			
	$\overline{K}_{23}$	11.2	11.2	12	10.7	$\overline{T}_3 = 3.77$		
	$\overline{K}_{33}$	8.9	10.2	10.5	11.7			
	R_3	1.63	0.77	0.5	0.33			

Analysis of the range value $R_i(i = 1 \sim 3)$ in Table 8 of the orthogonal test yielded that cam clearance A had the greatest effect on picking efficiency and harvesting rate of ripe fruit; the shedding rate of unripe fruit and the damaged fruit rate.

The following conclusions are obtained after analyzing and calculating $\overline{K}_{ij}(i = 1 \sim 3)$: the transmission clearance combination that can achieve the best picking efficiency of the harvester is $A_1B_1C_1F_3$; the transmission clearance combination that can achieve the lowest shedding rate of unripe fruit is $A_1B_1C_2F_1$; the transmission clearance combination that can achieve the lowest fruit damage rate is $A_1B_1C_2F_3$.In blueberry fruit harvesting operation, picking efficiency is the most important test index, followed by the damaged fruit rate and shedding rate of unripe fruit, thus the weight sequence of test indexes is obtained as follows: $Y_1 > Y_3 > Y_2$.

After analyzing the test factors A and B by combining the frequency of occurrence and $\overline{K}_{ij}(i = 1 \sim 3)$, A_1B_1 are the best transmission clearances for the cam clearance A and slider clearance B. Since $Y_1 > Y_3 > Y_2$, C_1 is the best transmission clearance for the left clearance B;and as the corresponding weight Y_2 is the lowest, F_3 is selected to be the best transmission clearance for the right clearance F.

Thus, the transmission clearance combination to achieve the best quality of harvested fruit and picking efficiency is: $A_1B_1C_1F_3$, in other words, cam clearance A is 0.25 mm, slider clearance B is 0.2 mm, left clearance C is 0.1 mm and right clearance F is 0.2 mm.

In order to realize the optimal design of the harvesting device parameters and give full play to the working performance of the machinery, blueberry picking test was conducted with the best combination of transmission clearance.

The picking efficiency and picked fruit's quality of the machine with the best combination of parameters were obtained: picking efficiency is 3.93 kg min^{-1}, shedding rate of unripe fruit is 3.1 % and fruit damage rate is 2.8 %, which was better than the test data of

groups in Table 7, and the results of the orthogonal test analysis could be used as the final design parameters of the harvester.

4. Conclusions

Firstly, the working principle of the blueberry picker and the mechanical structure of the picking system were analyzed, and the transmission clearance of the picking device was modeled by MLSD method. The collision force of transmission clearance of the picking device was analyzed in ADAMS and MATLAB respectively. And the dynamic simulation curves in ADAMS and the programming curves in MATLAB were obtained through comparison and analysis by *F*-test method. There was no significant difference between the two methods. The MLSD method used in this paper was suitable for modeling and analyzing the transmission clearance of blueberry picking device.

Secondly, ADAMS software was used to analyze the clearance force, the output torque of the combs and the fruit picking force under different transmission clearances. The results showed that the clearance force was proportional to the size of the transmission clearance; the output torque of the combs and the picking force of the blueberry fruit were inversely proportional to the transmission clearance. A self-developed blueberry picker was used for the field picking test. The influence of transmission clearance on picked fruit quality and picking efficiency of the machine and the software simulation results were enriched and improved were analyzed by linear regression method. With the increase of the transmission clearance of the slider clearance pair *B*, the picking efficiency of the machine, the shedding rate of unripe fruit and the damaged fruit rate showed a trend of increasing and then decreasing. And the maximum was reached when the clearance of the slider clearance pair *B* was 0.4 mm. The transmission clearance of other motion pairs is proportional to the picking efficiency of the machine, the shedding rate of unripe fruit and the damaged fruit rate.

Orthogonal test method was used to analyze the influence of different transmission clearance combinations on the picking efficiency and picked fruit quality of the machine. The optimal transmission clearance combinations of the device were as follows: cam clearance pair *A* was 0.25 mm, slider clearance pair *B* was 0.2 mm, left connecting rod pair *C* was 0.1 mm and right connecting rod pair *F* was 0.2 mm. The picking efficiency of the machine was 3.93 kg min^{-1}, the shedding rate of unripe fruit was 3.1 %, and the fruit damage rate of was 2.8 %.

The research results of this paper can provide a theoretical basis for the design of fruit picking machinery, so as to promote the development of China's blueberry picking mechanization.

Funding statement

This work was supported by the Harbin Science and Technology Bureau [grant numbers CXRC20231115883]; the China Postdoctoral Science Foundation [grant numbers 2019T120248]; and the Ministry of Education of the People's Republic of China [grant numbers 2572022DP01].

CRediT authorship contribution statement

Xiaomeng Lyu: Writing – review & editing, Writing – original draft, Visualization, Validation, Software, Methodology, Formal analysis, Conceptualization. **Haibin Wang:** Validation, Supervision, Software, Resources, Project administration, Methodology, Funding acquisition, Conceptualization. **Guangfei Xu:** Visualization, Validation, Software, Data curation. **Cun Chu:** Investigation, Data curation.

Declaration of competing interest

The authors declare that they have no known competing financial interests or personal relationships that could have appeared to influence the work reported in this paper.

Acknowledgments

We would also like to thank Prof. Li Zhipeng and Prof. Guo Yanling from the College of Mechanical and Electrical Engineering of Northeast Forestry University for their guidance and advice on the project.

References

[1] T. Xue, X. Yuan, J.L. Feng, R.H. Lin, Y.C. Chen, Optimization of the extraction process parameters of blueberry anthocyanin by response surface method, J. Fujian Normal Univ. (Philos. Soc. Sci. Ed.) 32 (1) (2016) 71–77 (In Chinese with English Abstract).

[2] Y.D. Bao, Z.P. Li, Y.L. Guo, H.B. Wang, Effects of vibrating based picking machine on blueberry fruit harvest, Journal of Hunan Agricultural University (Natural Sciences) 40 (1) (2014) 96–100 (In Chinese with English Abstract).

[3] L.W. Zhang, H.B. Wang, S. Li, F.H. Wang, Calibration of Discrete Element Model Parameters for Blueberry Based on Response Surface Methodology, vol. 51, J. Shenyang Agric. Univ., 2020, pp. 540–548 (In Chinese with English Abstract).

[4] L. Yang, J.F. Yang, Z.X. Hou, Z.Z. Gong, C. Wang, W.J. Shi, Effects of UV-B treatment on the major quality of blueberry and related enzyme activities in different development stages, Acta Bot. Boreali Occident. Sin. 35 (12) (2015) 2477–2482 (In Chinese with English Abstract).

[5] Y.D. Bao, Y.L. Guo, H. Zhang, S. Guo, Simulation and analysis of fruits collision during blueberry harvest based on ADAMS, Journal of Central South University of Forestry & Technology 33 (12) (2013) 157–160 (In Chinese with English Abstract).

[6] F. Takeda, W.Q. Yang, C. Li, A. Freivalds, K. Sung, R. Xu, B. Hu, J. Williamson, S. Sargent, Applying new technologies to transform blueberry harvesting, Agronomy 7 (2) (2017) 33, https://doi.org/10.3390/agronomy7020033.

[7] L. Brondino, D. Borra, N.R. Giuggioli, S. Massaglia, Mechanized blueberry harvesting: preliminary results in the Italian context, Agriculture 11 (12) (2021) 1197, https://doi.org/10.3390/agriculture11121197.

[8] P.C. Yu, C.Y. Li, F. Takeda, G. Krewer, G. Rains, T. Hamrita, Quantitative evaluation of a rotary blueberry mechanical harvester using a miniature instrumented sphere, Comput. Electron. Agric. 88 (2012) 25–31, https://doi.org/10.1016/j.compag.2012.06.005.

[9] S.A. Sargent, F. Takeda, J.G. Williamson, A.D. Berry, Harvest of southern highbush blueberry with a modified, over-the-row mechanical harvester: use of handheld shakers and soft catch surfaces, Agriculture 10 (2020) 4, https://doi.org/10.3390/agriculture10010004.

[10] S.A. Sargent, F. Takeda, J.G. Williamson, A.D. Berry, Harvest of southern highbush blueberry with a modified, over-the-row mechanical harvester: use of soft-catch surfaces to minimize impact bruising, Agronomy 11 (2021) 1412, https://doi.org/10.3390/agronomy11071412.

[11] H.B. Wang, X.M. Lv, F. Xiao, L.L. Sun, Analysis and testing of rigid–flexible coupling collision harvesting processes in blueberry plants, Agriculture 12 (2022) 1900, https://doi.org/10.3390/agriculture12111900.

[12] C.S. Fan, Z.P. Li, Y.L. Guo, The design and test of the northern high bush blueberry picking machine, Energy Conserv. Technol. 32 (1) (2014) 83–86+91 (In Chinese with English Abstract).

[13] Y.D. Bao, Y.L. Guo, S. Guo, Research progress of harvest technology and machinery of blueberry, Energy Conserv. Technol. 32 (3) (2014) 228–230 (In Chinese with English Abstract).

[14] J.R. Monique, R.S. Cesar, E.J. David, et al., Assessing the impact of cultivation and plant domestication of highbush blueberry (Vaccinium corymbosum) on soil properties and associated plant-parasitic nematode communities, Soil Biol. Biochem. 88 (2015) 25–28.

[15] C. Vanessa, G.V. Amadeo, L.M. José, et al., Influence of genotype, cultivation system and irrigation regime on antioxidant capacity and selected phenolics of blueberries (Vaccinium corymbosum L.), Food Chem. 202 (2016) 276–283.

[16] P. Flores, Modeling and simulation of wear in revolute clearance joints in multibody systems, Mech. Mach. Theor. 44 (6) (2009) 1211–1222, https://doi.org/10.1016/j.mechmachtheory.2008.08.003.

[17] J.L. Li, H.Z. Huang, S.Z. Yan, Y.Q. Yang, Kinematic accuracy and dynamic performance of a simple planar space deployable mechanism with joint clearance considering parameter uncertainty, Acta Astronaut. 136 (2017) 34–45, https://doi.org/10.1016/j.actaastro.2017.02.027.

[18] J.L. Li, S.Z. Yan, F. Guo, P.F. Guo, Effects of damping, friction, gravity, and flexibility on the dynamic performance of a deployable mechanism with clearance, Proc. IME C J. Mech. Eng. Sci. 227 (8) (2013) 1791–1803, https://doi.org/10.1177/0954406212469563.

[19] H.Y. Tan, Y.J. Hu, L. Li, Effect of friction on the dynamic analysis of slider-crank mechanism with clearance joint, Int. J. Non Lin. Mech. 115 (2019) 20–40, https://doi.org/10.1016/j.ijnonlinmec.2019.04.009.

[20] O. Muvengei, J. Kihiu, B. Ikua, Dynamic analysis of planar multi-body systems with LuGre friction at differently located revolute clearance joints, Multibody Syst. Dyn. 28 (2012) 369–393, https://doi.org/10.1007/s11044-012-9309-8.

[21] S. Akehurst, N.D. Vaughan, D.A. Parker, D. Simner, Modelling of loss mechanisms in a pushing metal V-belt continuously variable transmission. Part 1: torque losses due to band friction, Proc. Inst. Mech. Eng. - Part D J. Automob. Eng. 218 (11) (2004) 1269–1281, https://doi.org/10.1243/0954407042580020.

[22] S.F. Xiao, B. Chen, Q. Du, J. Mo, Vibration characteristics of the structure with CHEARANCES, Journal of Dynamics and Control 1 (2003) 35–40 (In Chinese with English Abstract).

[23] E. Zakhariev, Dynamics of rigid multibody systems with clearances in the joints, Mech. Struct. Mach. 27 (1) (1999) 63–87.

[24] O. Bauchau, J. Rodriguez, Modeling of joints with clearance in flexible multibody systems, Int. J. Solid Struct. 39 (1) (2002) 41–63.

[25] J.T. Ming, H.L. Tien, Kinematic sensitivity analysis of linkage with joint clearance based on transmission quality, Mech. Mach. Theor. 39 (11) (2004) 1189–1206, https://doi.org/10.1016/j.mechmachtheory.2004.05.009.

[26] G. Etesami, M.E. Felezi, Z.N. Nariman, Optimal transmission angle and dynamic balancing of slider-crank mechanism with joint clearance using Pareto Bi-objective Genetic Algorithm, J. Braz. Soc. Mech. Sci. Eng. 43 (4) (2021) 185–203, https://doi.org/10.1007/s40430-021-02834-8.

[27] Z.F. Bai, X. Jiang, F. Li, J.J. Zhao, Y. Zhao, Reducing undesirable vibrations of planar linkage mechanism with joint clearance, J. Mech. Sci. Technol. 32 (2018) 559–563, https://doi.org/10.1007/s12206-018-0103-7.

[28] Z.F. Bai, J.J. Zhao, J. Chen, Y. Zhao, Design optimization of dual-axis driving mechanism for satellite antenna with two planar revolute clearance joints, Acta Astronaut. 144 (2018) 80–89, https://doi.org/10.1016/j.actaastro.2017.11.015.

[29] C.Y. Ji, C. Zhang, B.X. Gu, H.J. Fu, D. Xie, J. Guo, Design and experiment of shear-sucting mountain Chrysanthemum picking machine, Trans. Chin. Soc. Agric. Mach. 48 (11) (2017) 137–145 (In Chinese with English Abstract).

[30] Y. Hayasaka, N. Okamoto, Analysis of nonlinear vibration of space apparatuses connected with pin-joints, Transactions of the Japan Society of Mechanical Engineers 59 (563) (1992) 2007–2014.

[31] S.L. Folkman, E.A. Rowsell, G.D. Ferney, Influence of pinned joints on damping and dynamic behavior of a truss, J. Guid. Control Dynam. 18 (6) (1995) 1398–1403.

[32] S. Dubowsky, F. Freudenstein, Dynamic analysis of mechanical systems with clearances, Part 2: dynamic response, J. Manuf. Sci. Eng. 93 (1) (1971) 310–316.

[33] S. Dubowsky, T.N. Gardner, Dynamic interactions of link elasticity and clearance connections in planar mechanical systems, Journal of Engineering for Industry 97 (2) (1975) 652–661.

[34] T. Furuhashi, N. Morita, M. Matsuura, Research on dynamics of four–bar linkage with clearances at turning pairs (4th report, forces acting at joints of crank–lever mechanism), Bulletin JSME 21 (1978) 1299–1305.

[35] T. Furuhashi, N. Morita, M. Matsuura, Research on dynamics of four-bar linkage with clearances at turning pairs, Bull.JSME 21 (1978) 518–523.

[36] G.Q. Wang, H.Z. Liu, C.A. He, Application of nonlinear contact model in chaos analysis of a mechanism with clearance joints, Mechanical Science and Technology for Aerospace Engineering 6 (2005) 636–638 (In Chinese with English Abstract).

[37] S.Z. Yan, B.Q. Liu, Y.W. Liu, T.Q. Huang, Dynamics of Flexible Multibody Systems-The Finite Segment Method, vol. 3, Journal of Hebei University of Technology, 1997, pp. 1–9 (In Chinese with English Abstract).

[38] D.L. Wu, Y. Wang, R. Wen, Some problems on the dynamics of large deployable mechanisms for space station, Chin. Space Sci. Technol. 6 (1996) 29–38 (In Chinese with English Abstract).

[39] T.S. Li, X.Y. Gou, Study on dynamics of a rigid-flexible coupling system with backlash hinges, Chin. Space Sci. Technol. 1 (2000) 15–19 (In Chinese with English Abstract).

[40] Y.J. Jiang, Y.T. Liao, C. Qin, Z.H. Guan, Q.X. Liao, Vibration analysis and improvement for frame of 4SY-2.9 typed tape windrower, Trans. Chin. Soc. Agric. Eng. 33 (9) (2017) 53–60 (In Chinese with English Abstract).

[41] H.T. Li, X.Y. Wan, Y. Xu, Clearance adaptive adjusting mechanism for header screw conveyor of rape combine harvester, Trans. Chin. Soc. Agric. Mach. 48 (11) (2017) 115–122 (In Chinese with English Abstract).

[42] H.X. Yao, A Theoretical Study on Mechanism Dynamics with Muti-Clearances, XIANGTAN UNIVERSITY, Hu Nan, China, 2014 (In Chinese with English Abstract).

[43] B.X. Liu, H.X. Yao, S.H. Nie, Parameter identification of LuGre friction model based on interval analysis, China Mech. Eng. 24 (19) (2013) 2647–2651 (In Chinese with English Abstract).

[44] P.Z. He, H. Zhu, Y.L. Guo, Y.D. Bao, L.L. He, Simulation of blueberry picking institution based on ADAMS, Mod. Sci. Instrum. 29 (2012) 36–38+42 (In Chinese with English Abstract).

[45] L. Shi, J.C. Fan, H. Qiao, Design and simulation of blueberry picking mechanism based on the ADAMS, Mech. Res. Appl. 28 (2015) 158–160 (In Chinese with English Abstract).

[46] L.W. Zhang, H.B. Wang, S. Li, F.H. Wang, Calibration of Discrete Element Model Parameters for Blueberry Based on Response Surface Methodology, vol. 51, J. Shenyang Agric. Univ., 2020, pp. 540–548 (In Chinese with English Abstract).

[47] Z. Wang, L.L. Gu, Z.Z. Gao, B. Liu, Y.L. Wang, Experimental study on Poisson's ratio of lumber by dynamic testing, Sci. Silvae Sin. 51 (2015) 102–107 (In Chinese with English Abstract).
[48] R.L. Wang, X.H. Bai, J.W. Qin, The single factor experimental design and analysis of agricultural machinery, Agric. Sci. Technol. Equip. 9 (2014) 26–28+31 (In Chinese with English Abstract).
[49] L.Z. Xu, Y.M. Li, Finite element analysis on damage of rice kernel impacting on spike tooth, Trans. Chin. Soc. Agric. Eng. 27 (2011) 27–32 (In Chinese with English Abstract).
[50] N.L. Zheng, H. Zhang, Y. Zhu, Dynamic modeling and simulation of flexible multi-link mechanism including joints with clearance for ultra-precision press, Trans. Chin. Soc. Agric. Mach. 48 (1) (2017) 375–385 (In Chinese with English Abstract).
[51] J.J. Ying, Y.H. Chen, K. He, J.Z. Liu, Design and experiment of grape-picking device with grasping and rotary-cut type of underactuated double fingered hand, Trans. Chin. Soc. Agric. Mach. 48 (11) (2017) 12–20 (In Chinese with English Abstract).
[52] L. Dong, W.C. Tang, C. Liu, Modeling and analysis of flexible ball screw driven servomechanisms with friction and backlash, Trans. Chin. Soc. Agric. Mach. 44 (11) (2013) 300–307 (In Chinese with English Abstract).
[53] Y.F. Qi, H.D. Xu, L.H. Wang, Frictional impact dynamics model of threshing process between flexible teeth and grains, J. Jilin Univ. (Eng. Technol. Ed.) 27 (2011) 19–22 (In Chinese with English Abstract).
[54] H. Wang, W. Wang, The frictional self-excited vibration of machine tool, J. Yantai Univ. (Nat. Sci. Eng.) 10 (1997) 59–65 (In Chinese with English Abstract).